Alpine lee cyclogenesis influence on air-sea heat exchanges and marine atmospheric boundary layer thermodynamics over the western Mediterranean during a Tramontane/Mistral event

Cyrille Flamant

▶ **To cite this version:**

Cyrille Flamant. Alpine lee cyclogenesis influence on air-sea heat exchanges and marine atmospheric boundary layer thermodynamics over the western Mediterranean during a Tramontane/Mistral event. Journal of Geophysical Research. Oceans, 2003, 108 (C2), 10.1029/2001JC001040 . hal-04110042

HAL Id: hal-04110042
https://hal.science/hal-04110042

Submitted on 5 Jun 2023

HAL is a multi-disciplinary open access archive for the deposit and dissemination of scientific research documents, whether they are published or not. The documents may come from teaching and research institutions in France or abroad, or from public or private research centers.

L'archive ouverte pluridisciplinaire **HAL**, est destinée au dépôt et à la diffusion de documents scientifiques de niveau recherche, publiés ou non, émanant des établissements d'enseignement et de recherche français ou étrangers, des laboratoires publics ou privés.

Copyright

JOURNAL OF GEOPHYSICAL RESEARCH, VOL. 108, NO. C3, 8057, doi:10.1029/2001JC001040, 2003

Alpine lee cyclogenesis influence on air-sea heat exchanges and marine atmospheric boundary layer thermodynamics over the western Mediterranean during a Tramontane/Mistral event

Cyrille Flamant

Service d'Aéronomie/IPSL, Université Pierre et Marie Curie, Paris, France

Received 26 June 2001; revised 4 February 2002; accepted 11 February 2002; published 11 February 2003.

[1] Data from a recent field campaign are used to analyze the nonstationary aspects of air-sea heat exchanges and marine atmospheric boundary layer (MABL) thermodynamics over the Gulf of Lion (GoL) in connection with synoptic forcing. The data set includes measurements made from a wide range of platforms (sea-borne, airborne, and space-borne) as well as three-dimensional atmospheric modeling. The analysis focuses on the 24 March 1998 Tramontane/Mistral event. It is shown that the nonstationary nature of the wind regime over the GoL was controlled by the multistage evolution of an Alpine lee cyclone over the Tyrrhenian Sea (between Sardinia and continental Italy). In the early stage (low at 1014 hPa) the Tramontane flow prevailed over the GoL. As the low deepened (1010 hPa), the prevailing wind regime shifted to a well-established Mistral that peaked around 1200 UTC. In the afternoon the Mistral was progressively disrupted by a strengthening outflow coming from the Ligurian Sea in response to the deepening low over the Tyrrhenian Sea (1008 hPa) and the channelling induced by the presence of the Apennine range (Italy) and the Alps. In the evening the Mistral was again well established over the GoL as the depression continued to deepen (1002 hPa) but moved to the southeast, reducing the influence of outflow from the Ligurian Sea on the flow over the GoL. The air-sea heat exchanges and the structure of the MABL over the GoL were observed to differ significantly between the established Mistral period and the disrupted Mistral period. In the latter period, surface latent and sensible heat fluxes were reduced by a factor of 2, on average. During that latter period, air-sea moisture exchanges were mainly driven by dynamics, whereas during the former period, both winds and vertical moisture gradients controlled moisture exchanges. The MABL was shallower during the latter period (0.7 km instead of 1.2 km) because of reduced surface turbulent heat fluxes and increased wind shear at the top of the MABL in connection with the outflow from the Ligurian Sea. In the period of established Mistral, gravity waves above the MABL were observed to have an influence on the MABL structure. In the perturbed Mistral case this influence was not observed. Over the GoL the ubiquitous presence of sheltered regions (i.e., regions of reduced wind speed in the MABL) in the lee of the three major mountain ranges surrounding the GoL (namely, the Pyrénées, the Massif Central, and the Alps) was shown to have an impact on surface turbulent heat fluxes. The position of these sheltered regions, which evolved with the synoptic conditions, was the key to a correct interpretation of multiplatform surface turbulent flux measurements made over the GoL on 24 March 1998. *INDEX TERMS:* 3329 Meteorology and Atmospheric Dynamics: Mesoscale meteorology; 3307 Meteorology and Atmospheric Dynamics: Boundary layer processes; 3339 Meteorology and Atmospheric Dynamics: Ocean/atmosphere interactions (0312, 4504); 3360 Meteorology and Atmospheric Dynamics: Remote sensing; 3337 Meteorology and Atmospheric Dynamics: Numerical modeling and data assimilation; *KEYWORDS:* atmospheric boundary layer, lidar, Alpine lee cyclogenesis, mistral, numerical prediction model, Gulf of Lion

Citation: Flamant, C., Alpine lee cyclogenesis influence on air-sea heat exchanges and marine atmospheric boundary layer thermodynamics over the western Mediterranean during a Tramontane/Mistral event, *J. Geophys. Res.*, *108*(C3), 8057, doi:10.1029/2001JC001040, 2003.

Copyright 2003 by the American Geophysical Union.
0148-0227/03/2001JC001040

1. Introduction

[2] It is now well accepted that the next step toward a noticeable improvement in understanding coastal meteorology will be achieved through the use of a coupled ocean-atmosphere model in coastal regions. Such models already exist [*Hodur*, 1997; *Powers and Stoeling*, 2000; *Estournel et al.*, 2003] but have yet to be thoroughly tested and validated. As air-sea exchanges are key in driving both the atmospheric and oceanic circulations, mesoscale turbulent heat flux fields over coastal waters are desperately needed for such validation exercises. As a result, the development of instruments and methodologies to measure turbulent heat flux from sea-borne, ship-borne, and airborne platforms has become increasingly important in recent years. However, the representativity of such measurements is very difficult to assess at the mesoscale because of the variety of forcings driving the fluxes as well as the scales at which their influence is most efficient. Among the most important forcings we find sea state, wind conditions and the response of the marine atmospheric boundary layer (MABL) to external mesoscale or synoptic forcing.

[3] In this paper, we use the turbulent heat flux measurements made from a still buoy, a ship and an aircraft over the Gulf of Lion (GoL), western Mediterranean, during the 24 March 1998 Mistral/Tramontane wind event documented in the framework of the FETCH (Flux, État de mer et Télédétection en Condition de fetcH variable) experiment [*Hauser et al.*, 2000, 2003] to discuss these representativity issues. The Tramontane and the Mistral are low level, orography-induced, cold air outbreaks over the GoL blowing offshore of Narbonne and Arles, France, respectively (Figure 1). They are frequently observed to extend several hundreds of kilometers from the coast, bringing cold and dry continental air over the warm western Mediterranean, and hence, generating intense heat air-sea exchanges. They are one of the primary cause of storms over the Mediterranean, between Italy and the Balearic Islands [*Trigo et al.*, 1999; *Campins et al.*, 2000].

[4] An important part of the paper is dedicated to the analysis of the spatiotemporal evolution of turbulent heat flux measurements in the synoptic and mesoscale context provided by forecasts from the operational model ALADIN of Météo-France. Emphasis is put on the nonstationary nature of the Tramontane/Mistral wind regime over the GoL on 24 March 1998 which was controlled by the evolution of an Alpine lee cyclone over the Tyrrhenian Sea (between Sardinia and continental Italy).

[5] The paper is organized as follows. In section 2, we briefly describe the objectives of the FETCH experiment as well as the operations which took place on 24 March 1998 over the GoL. In section 3, we briefly present the numerical weather prediction model ALADIN used in this study. In section 4, we discuss the evolution of the synoptic situation over the Mediterranean on 24 March 1998, based on ALADIN simulations. We show that at least three wind regimes (namely Tramontane, established Mistral and disrupted Mistral) prevailed over the GoL in response to the different stages of development of the cyclone. In section 5, we present a mesoscale analysis of the MABL thermodynamics over the GoL, in the region of the FETCH experiment operations. Emphasis is put on the ubiquitous presence

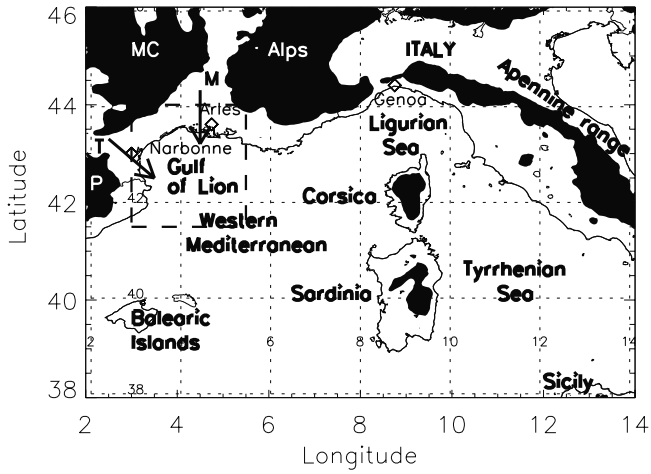

Figure 1. Presentation of the Northern Mediterranean region showing the location of the geographical features referred to in this paper. Shaded areas correspond to the topography above 500 m: the Pyrénées (P), the Massif Central (MC), the Alps, and the Apennine range (mountains are also seen in Corsica and Sardinia). The dashed box indicates the FETCH domain within which two aircraft, a ship, and a buoy were deployed. The thick arrows indicate the climatological directions of the Mistral (M) and Tramontane (T) winds.

over the Mediterranean of sheltered regions (i.e., regions of reduced wind speed in the MABL) in the lee of the three major mountain ranges surrounding the GoL (namely, the Pyrénées, the Massif Central and the Alps, see Figure 1) and their impact on surface turbulent heat fluxes. The spatio-temporal evolution of mean and turbulent variables measured from a buoy, a ship and two aircraft is then analyzed in section 6 on the basis of the mesoscale and synoptic-scale forcings. Finally, airborne lidar and in situ measurements are used to depict the structure of the MABL over the GoL (section 7). It is shown to differ significantly between the established Mistral period and the disrupted Mistral period. In section 8, summarize and conclude.

2. FETCH Experiment: Rationale and Operations on 24 March 1998

[6] The FETCH experiment [*Hauser et al.*, 2000, 2003] took place over the Mediterranean from 12 March to 15 April 1998 and was dedicated to the study of the interactions between the ocean and the atmosphere in a coastal environment under strong wind conditions. The period of the experiment was chosen for being favorable to Tramontane and Mistral events. As there is still a lot of uncertainties associated with the parameterization of the influence of sea state and MABL structure on surface turbulent fluxes, an airborne lidar and an airborne radar ocean wave spectrometer were flown in formation during FETCH (a first in such air-sea exchange-oriented field experiments) to document simultaneously the MABL structure and the sea state, respectively, at the mesoscale. These two aspects were thought primordial since the influence of the sea state on the fluxes and their parameterization is still subject to

21562202c, 2003, C2, Downloaded from https://agupubs.onlinelibrary.wiley.com/doi/10.1029/2001JC001040 by Cochrane France, Wiley Online Library on [05/06/2023]. See the Terms and Conditions (https://onlinelibrary.wiley.com/terms-and-conditions) on Wiley Online Library for rules of use; OA articles are governed by the applicable Creative Commons License

contradiction and controversy in the literature [see *Dupuis et al.*, 1997; *Eymard et al.*, 1999; W. M. Drennan et al., On the wave age dependence of wind stress over pure wind seas, submitted to *Journal of Geophysical Research*, 2002, hereinafter referred to as Drennan et al., submitted manuscript, 2002, and references therein], while very few studies deal with the impact of the MABL structure on turbulent fluxes [e.g., *Marht et al.*, 1998]. In this paper, only the latter aspect is dealt with. The influence of sea state is presented elsewhere (e.g., Drennan et al., submitted manuscript, 2002).

[7] Despite the 6 weeks allocated to FETCH, only 2 Tramontane/Mistral events occurred (14 March and 24 March 1998). In this paper, we focus on the 24 March 1998 case only. Four platforms were available for that event: two aircraft (the Avion de Recherche Atmosphérique et de Télédétection (ARAT) and the Merlin IV), the R/V *Atalante* and the Air-Sea Interaction Spar (ASIS) buoy [*Graber et al.*, 2000], located at 43°N/4.25°E. All platforms were equipped so to measure in situ mean meteorological variables and turbulent fluxes, with the exception of ASIS which only measured momentum fluxes. In the particular case of ASIS and the R/V *Atalante* these measurements were made at 7 and 17 m above sea level, respectively. The structure of the MABL was documented using the down looking differential absorption lidar LEANDRE 2 [*Bruneau et al.*, 2001a, 2001b] embarked on the ARAT as well as aircraft soundings and balloon soundings launched from the R/V *Atalante*.

[8] Two two-aircraft missions were performed on 24 March 1998. In both cases, the flight tracks were designed in such a manner that long levelled legs be flown along and across the mean MABL wind direction (for turbulent flux computation purposes). In the following, we focus almost entirely on ARAT measurements. Only turbulent flux measurements made by the Merlin in the morning (on the same track than the ARAT) were used. In the morning, the ARAT flew an L-shaped pattern (A-D-E, leg A-D being aligned with the mean wind) at 13000 ft ASL (Figure 2a and Figure 3.) from 1014 to 1053 UTC, with LEANDRE 2 pointing to the nadir in order to describe the evolution of the ABL structure. The ARAT then performed a sounding between E and D, before documenting the ABL at 100 m ASL and at 300 m ASL along legs DE and BC, with LEANDRE 2 pointing to the zenith, between 1110 and 1233 UTC. In the afternoon, the ARAT flew an X-shaped pattern (A-F-C-E, leg A-F being aligned with the mean wind) at 13000 ft ASL (Figure 2b) from 1620 to 1730 UTC, with LEANDRE 2 pointing to the nadir. The ARAT then performed a sounding between E and F, before documenting the ABL at 100 m ASL (F-B-C) and at 300 m ASL (C-B-A), with LEANDRE 2 pointing to the zenith, between 1750 and 1850 UTC. In the following, the morning and afternoon ARAT flights are referred to as F02 and F03, respectively. The R/V *Atalante* track on 24 March 1998 is shown in Figure 2c. The position of the ASIS buoy is indicated by the diamond in Figure 2.

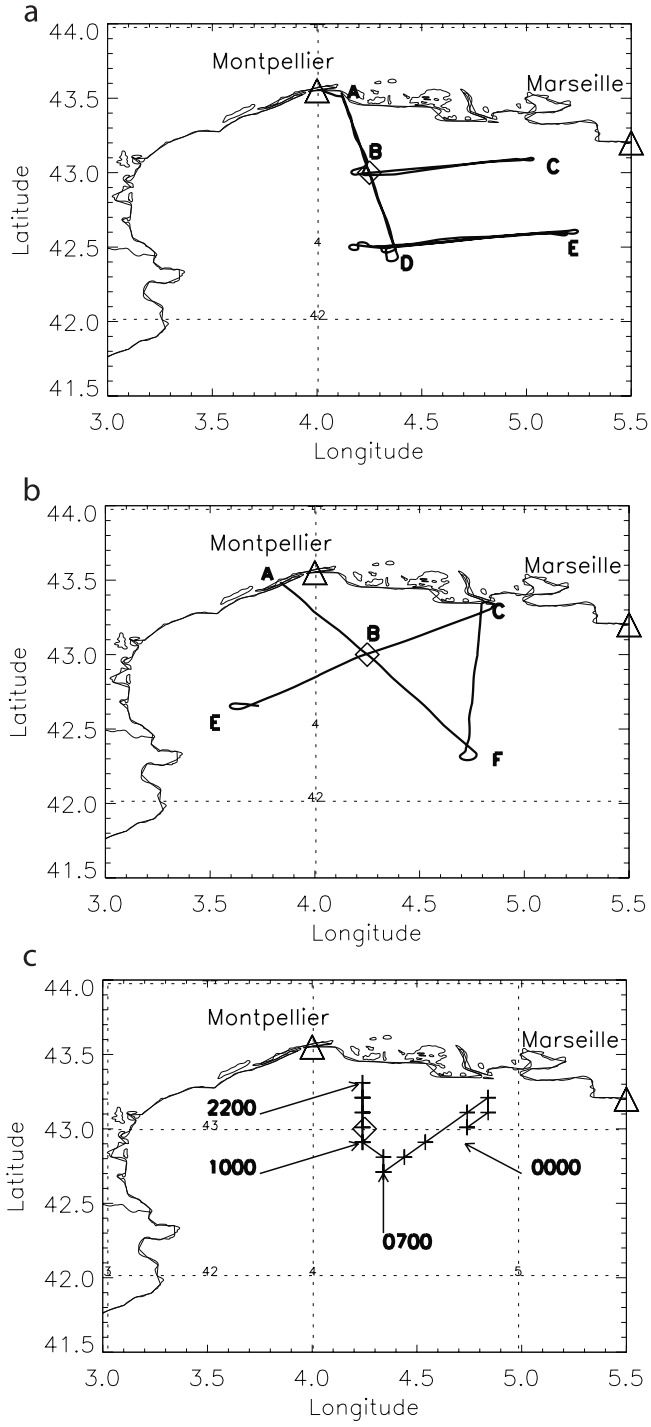

Figure 2. Flight tracks flown by the ARAT in the (a) morning and (b) afternoon of 24 March 1998. (c) The R/V *Atalante* track on that day is also shown. The labels (0000, 0700, . . .) indicate the time (UTC) at the location pointed to by each arrow. Crosses indicate hourly positions of the ship. Note that, at some periods, the ship did stay in the same location for more that an hour. Triangles indicate major cities, and the diamond indicates the position of the ASIS buoy.

3. Modeling Strategy

[9] In addition to the means specially deployed for FETCH, Météo-France provided daily forecasts of the meteorological situation made with the operational model ALADIN. ALADIN is a spectral limited area model, taking its boundary conditions from the global model ARPEGE of

21562202c, 2003, C2, Downloaded from https://agupubs.onlinelibrary.wiley.com/doi/10.1029/2001JC001040 by Cochrane France, Wiley Online Library on [05/06/2023]. See the Terms and Conditions (https://onlinelibrary.wiley.com/terms-and-conditions) on Wiley Online Library for rules of use; OA articles are governed by the applicable Creative Commons License

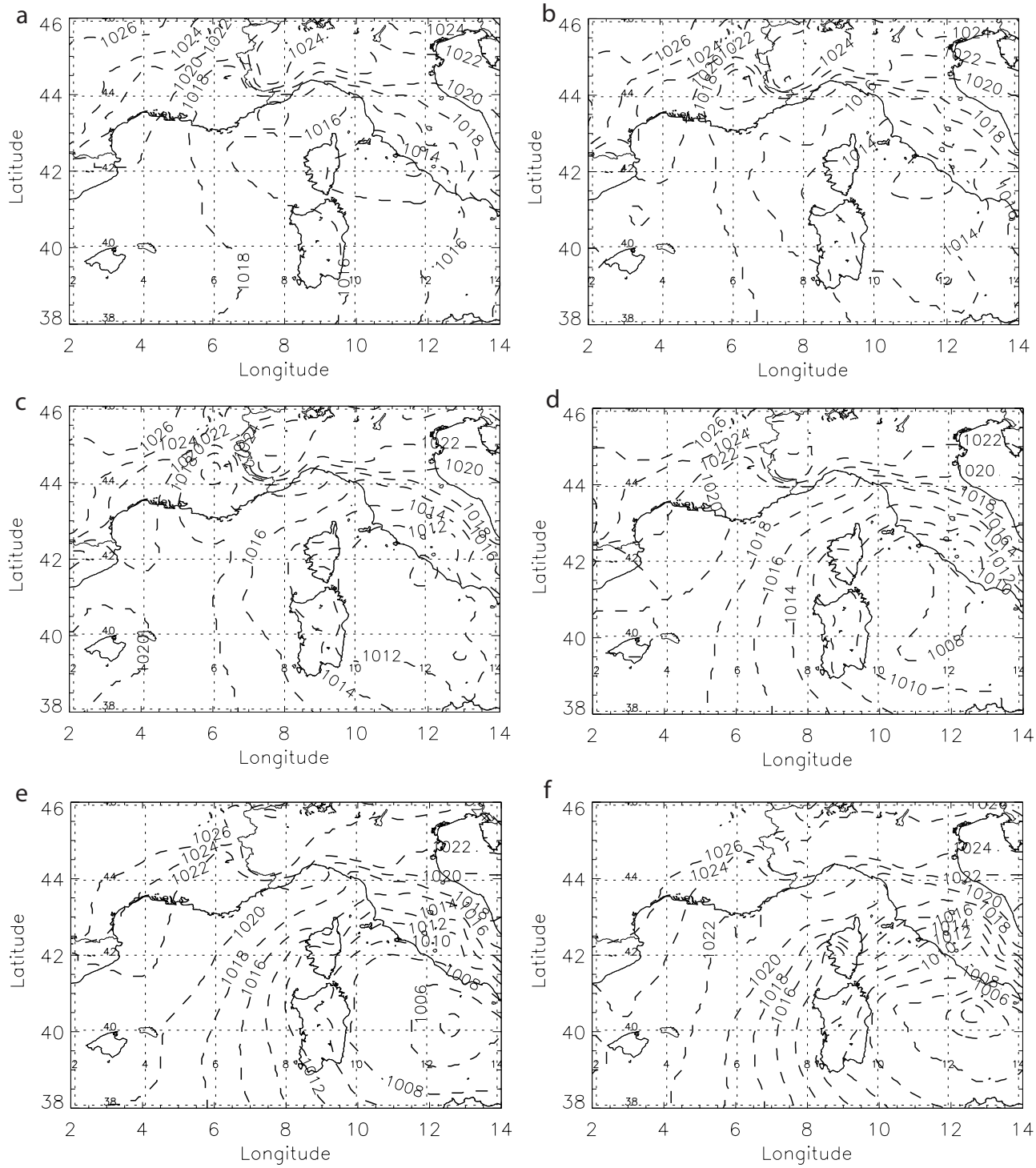

Figure 3. Sea surface pressure forecasted on 24 March 1998 by the French operational model ALADIN at (a) 0600, (b) 0900, (c) 1200, (d) 1500, (e) 1800, and (f) 2100 UTC. Sea surface isobars are between 1000 and 1026 hPa with 2 hPa increments.

Météo-France, which covers a domain of 2739 km × 2739 km (centered on France). The horizontal resolution is approximately 10 km, with 31 levels on the vertical, the highest level being at 5 hPa and the lowest level at approximately 17 m above ground/sea level. The surface layer and planetary boundary layer fluxes are computed on the lowest level using a modified version of the scheme developed by *Louis et al.* [1981]. The 3D-var data assimilation provides two analyses per day (0000 and 1200 UTC) but no associated first guess. Forecasts are available every 3 hour, i.e., at 0000, 0300, 0600, 0900, 1200, 1500, 1800, 2100 and 2400 UTC. Three hour integrated surface turbulent fluxes are computed from 12 hour forecasts. Additional information is given by *Eymard et al.* [2003].

21562202c, 2003, C2, Downloaded from https://agupubs.onlinelibrary.wiley.com/doi/10.1029/2001JC001040 by Cochrane France, Wiley Online Library on [05/06/2023]. See the Terms and Conditions (https://onlinelibrary.wiley.com/terms-and-conditions) on Wiley Online Library for rules of use; OA articles are governed by the applicable Creative Commons License

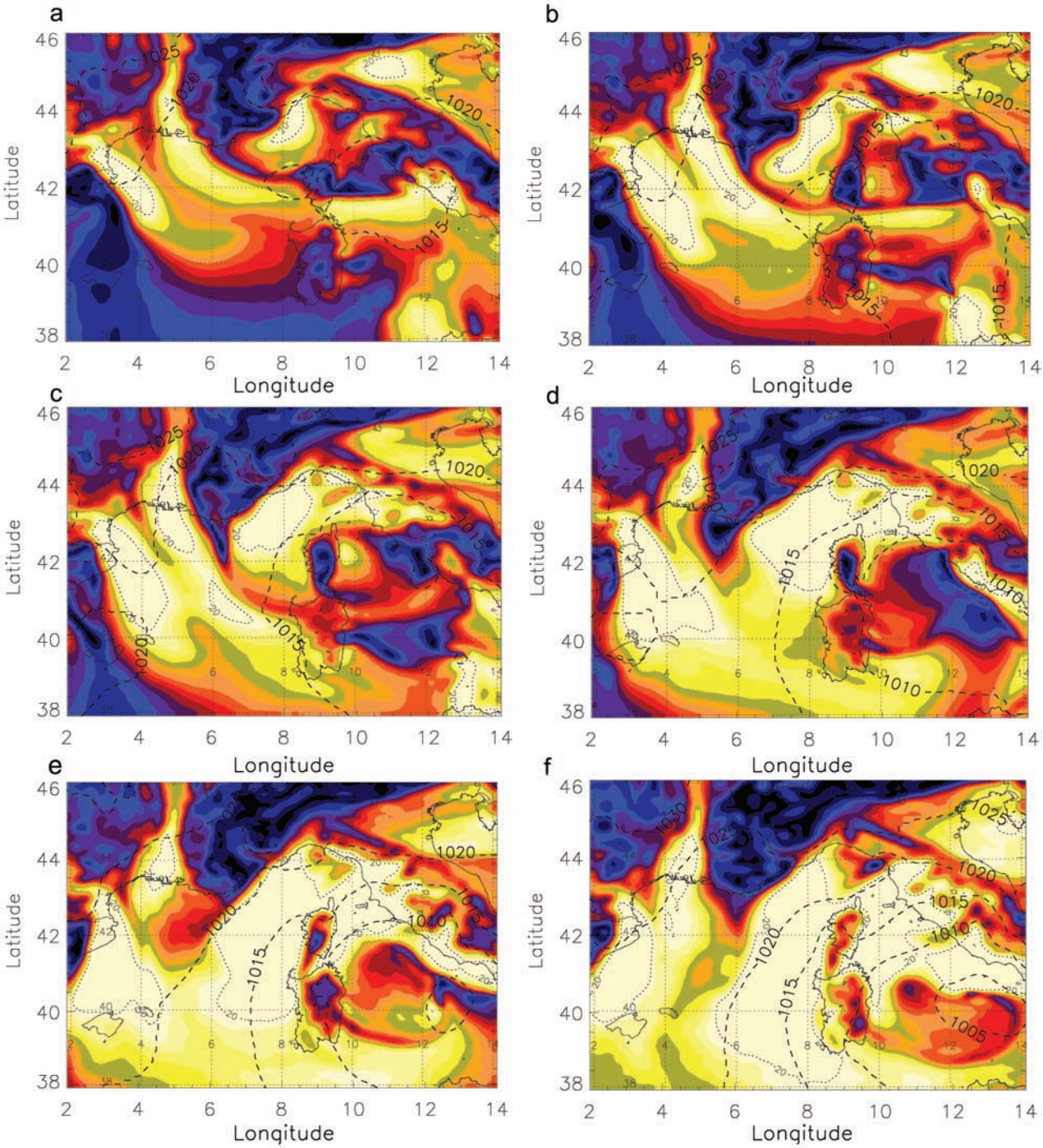

Figure 4. Wind speed field simulated in the ABL (at 950 hPa) on 24 March 1998 by the French operational forecast model ALADIN at (a) 0600, (b) 0900, (c) 1200, (d) 1500, (e) 1800, and (f) 2100 UTC. Superimposed are the sea surface isobars between 1000 and 1030 hPa with 5 hPa increments and the 20 m s^{-1} isotach. In the false color scale, blue/dark blue corresponds to wind speeds less than 5 m s^{-1}, and white corresponds to wind speeds equal to or larger than 20 m s^{-1}. Redish colors correspond to wind speeds of the order of 10 m s^{-1}.

[10] The forecasts products of interest for this study are: temperature, humidity and wind distributed on 16 pressure levels between 1000 and 100 hPa (namely, 1000, 950, 925, 900, 850, 800, 750, 700, 600, 500, 400, 300, 250, 200, 150, and 100 hPa). Sea level pressure and surface turbulent fluxes are provided at the lowest level, i.e., 17 m ASL. Near surface extrapolated fields (at 10 m ASL for the wind and 2 m ASL for temperature and humidity) are derived assuming a neutral profile. The SST in the model is issued from Reynolds' climatology and yields characteristic spatial and temporal scales of about 2° and 8 days.

215622022c, 2003, C2, Downloaded from https://agupubs.onlinelibrary.wiley.com/doi/10.1029/2001JC001040 by Cochrane France, Wiley Online Library on [05/06/2023]. See the Terms and Conditions (https://onlinelibrary.wiley.com/terms-and-conditions) on Wiley Online Library for rules of use; OA articles are governed by the applicable Creative Commons License

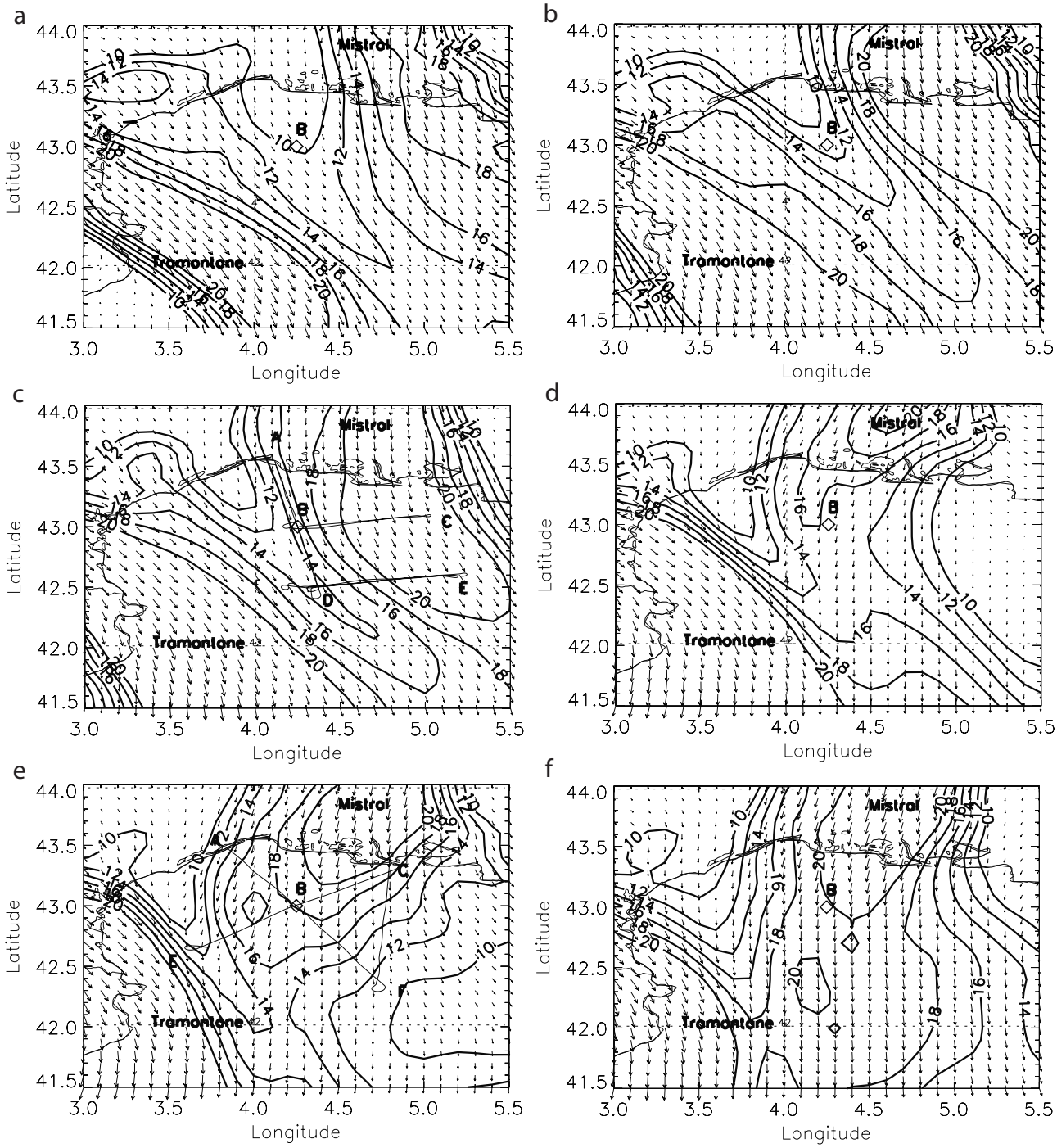

Figure 5. Wind fields simulated in the ABL (at 950 hPa) on 24 March 1998 by the French operational forecast model ALADIN at (a) 0600, (b) 0900, (c) 1200, (d) 1500, (e) 1800, and (f) 2100 UTC. The diamond corresponds to the position of the ASIS buoy. Superimposed are isotachs between 10 and 20 m s^{-1} with 2 m s^{-1} increments. Also superimposed on wind fields at 1200 and 1800 UTC are the ARAT flight tracks corresponding to the morning and afternoon flights (F02 and F03), respectively. The rugged solid line represents the coastline.

[11] In the framework of FETCH, forecasts were used as tools for (i) deciding whether or not to start an intensive observation period (IOP) and (ii) designing flight plans for aircraft and routes for the R/V *Atalante*. An ancillary objective for Météo-France was to confront ALADIN forecasts to multiplatform measurements during these IOPs in a region where such measurements are sparse.

[12] A thorough comparison of ALADIN forecasts and aircraft in situ measurements was conducted on 4 meteorological variables: wind speed, wind direction, humidity and temperature in order to determine which ALADIN forecasts better depicted the flow over the GoL at the time of the flights. This was done for ABL measurements (see Appendix) as well as high level measurements. These comparisons show that the

215622022c, 2003, C2, Downloaded from https://agupubs.onlinelibrary.wiley.com/doi/10.1029/2001JC001040 by Cochrane France, Wiley Online Library on [05/06/2023]. See the Terms and Conditions (https://onlinelibrary.wiley.com/terms-and-conditions) on Wiley Online Library for rules of use; OA articles are governed by the applicable Creative Commons License

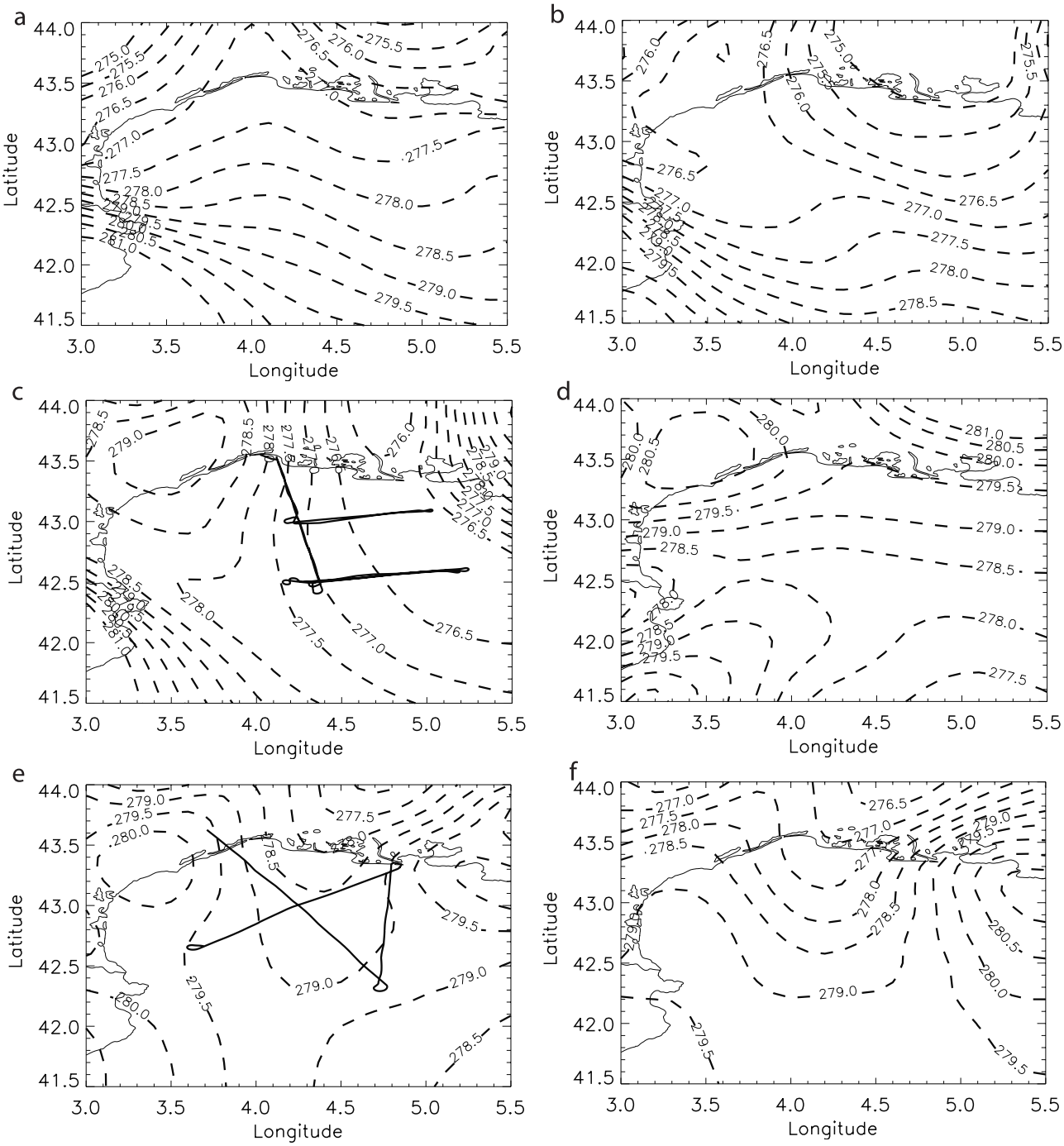

Figure 6. Temperature fields forecasted in the ABL (at 950 hPa) on 24 March 1998 by the French operational model ALADIN at (a) 0600, (b) 0900, (c) 1200, (d) 1500, (e) 1800, and (f) 2100 UTC. Superimposed are isentropes between 275 and 281 K with 0.5 K increments. Also superimposed are the ARAT trajectories in the morning (1200 UTC fields) and in the afternoon (1800 UTC fields).

thermodynamical conditions prevailing over the GoL during the morning (afternoon) flight were well represented by the 1200 UTC (1800 UTC) ALADIN forecasts.

4. Synoptic-Scale Analysis

[13] The 24 March 1998 Tramontane/Mistral event was intimately linked to the existence of an upper level trough (and its associated cold front) progressing toward the Alps (not shown) and the presence of a shallow vortex (1014 hPa) over the Tyrrhenian Sea (between Sardinia and continental Italy) at 0600 UTC. As the day progressed, the low over the Tyrrhenian deepened (from 1014 to 1008 hPa between 0600 and 1500 UTC) while remaining relatively still. From 1500 UTC on, the low continued to deepen (from 1008 to 1002 hPa) while moving to the southeast. It was located over Sicily on 25 March 1998 at 0600 UTC (not shown, see Figure 1 for the location of the geographical features referred to in this paper).

215622022c, 2003, C2, Downloaded from https://agupubs.onlinelibrary.wiley.com/doi/10.1029/2001JC001040 by Cochrane France, Wiley Online Library on [05/06/2023]. See the Terms and Conditions (https://onlinelibrary.wiley.com/terms-and-conditions) on Wiley Online Library for rules of use; OA articles are governed by the applicable Creative Commons License

[14] This two-phase evolution of Alpine lee cyclogenesis has been observed before [*Egger*, 1972; *Buzzi and Tibaldi*, 1978]. *Alpert et al.* [1996] have shown that topographical blocking was the dominant factor in the first and most rapid phase of the cyclone deepening. During the second phase, the growth rate drops to baroclinic values and the structure of the cyclone approaches that of typical extratropical systems. Convection as well as sensible and latent heat fluxes play an important role in the second phase of Alpine lee cyclogenesis development [*Alpert et al.*, 1996; *Grotjahn and Wang*, 1989]. These authors have also shown that convection had a tendency to move the cyclone to the east-northeast while topography had a tendency to tie the cyclone to the lee of the Alps. The sea moisture fluxes tend to move the cyclone toward the warm bodies of water (i.e., toward Sicily in our case).

[15] The multistage evolution of the Alpine lee cyclone over the Tyrrhenian Sea induced a very nonstationary wind regime over the GoL (see following section). The diurnal evolution of the Tramontane and Mistral flows on 24 March 1998 are evidenced on the wind field simulated in the ABL (at 950 hPa) by the French operational forecast model ALADIN at 0600, 0900, 1200, 1500, 1800 and 2100 UTC (Figure 4). They are identified as cores of wind speed larger than 20 m s^{-1}.

[16] In the early stage (low at 1014 hPa, 0600 UTC), the Tramontane flow prevailed over the GoL. The large westerly flow component (leading to prevailing Tramontane conditions) resulted from the rather high position (in terms of latitude) of the depression. The Mistral extended all the way to Southern Corsica, wrapping around the depression. To the north, a weak easterly outflow was observed over the Gulf of Genoa. As the low deepened (1010 hPa), the prevailing wind regime shifted to a well-established Mistral which peaked around 1200 UTC. The Mistral was observed to reach Southern Sardinia where it wrapped up around the depression. At this time, the outflow from the Ligurian Sea (i.e., Gulf of Genoa) had become stronger. In the afternoon, the Mistral was progressively disrupted by the strengthening outflow coming from the Ligurian Sea in response to the deepening low over the Tyrrhenian Sea (1008 hPa, 1500 UTC) and the channelling induced by the presence of the Apennine range (Italy) and the Alps. In the evening, the Mistral was again well established over the GoL as the depression continued to deepen (1002 hPa, 2100 UTC) but moved to the southeast, reducing the influence of outflow from the Ligurian Sea on the flow over the GoL. Generally speaking, during this period, the Tramontane flow appeared to be much more steady than the Mistral and less disrupted by the return flow associated with the depression. The cold air outbreak episode over the GoL ended on 25 March at 0600 UTC and anticyclonic conditions then prevailed over the GoL.

[17] An important feature of the cold air outbreak over the GoL is also observed in the form of banners of weaker winds (sheltered region) separating (i) the Mistral and the Tramontane (in the lee of the Masif Central) and (ii) the Mistral and the Ligurian Sea outflow (in the lee of the Maritime Alps, see Figure 4). Such sheltered regions are a common feature over the Mediterranean due to the presence of numerous mountain ranges. This lee phenomenon is also intimately related to potential vorticity banners (i.e., regions of important wind shear) generated downstream of major mountain ranges [e.g., *Aebischer and Schär*, 1998]. In the particular case of the Alps, low-level potential vorticity has been shown to contribute to the deepening of Alpine lee cyclones [*Aebischer and Schr*, 1998].

5. Mesoscale Analysis

[18] In this section, we first analyze the diurnal evolution of the Tramontane/Mistral related cold air outbreak over the GoL in terms of ABL thermodynamics and surface turbulent fluxes. This is done using wind, relative humidity and temperature fields simulated in the ABL (at 950 hPa) by ALADIN at 0600, 0900, 1200, 1500, 1800 and 2100 UTC (Figures 5, 6, and 7, respectively). On the basis of this analysis, an interpretation of airborne and ship-borne turbulent fluxes in the mesoscale context is proposed in section 6.

5.1. Atmospheric Boundary Layer Thermodynamics

[19] Figure 5 presents a close up of the ALADIN wind field at 950 hPa over the GoL on 24 March 1998. The location of the sheltered region in the lee of the Massif Central was observed to shift southward during the course of the day. Over the GoL, this region was characterized by low wind speeds (on the order of 10 m s^{-1}, immediately in the lee of the obstacle) separating the Tramontane (to the southwest) from the Mistral (to the northeast). Depending on the synoptic conditions, the edges of this sheltered region are more or less sharply defined.

[20] At 0600 UTC, we observed a strong, well-established Tramontane regime, wind speeds reaching 24 m s^{-1} (Figure 5a). We also observed the sheltered region associated with the Pyrnnes in the southwesternmost part of the domain. In comparison, the Mistral flow was not as intense. The temperature distribution at 950 hPa was observed to be essentially zonal over the GoL, the influence of the Mistral being only felt in the eastern part of the domain (Figure 6a). Large relative humidities ($\approx$60%) were associated with both the Tramontane and the Mistral (Figure 7a). Even larger relative humidities (above 70%) were observed in a region where the Tramontane and the Mistral flow merged (i.e., at roughly 42°N/5.0°E).

[21] At 0900 UTC, the Mistral and the Tramontane were observed to be strong, both winds being characterized by core wind speeds of at least 20 m s^{-1} (Figure 5b). The characteristics of the Mistral (a cold and dry jet) are now observed in the northernmost part of the GoL. The temperatures and relative humidities associated with the Mistral are less than those associated with the Tramontane (Figure 6b and Figure 7b, respectively).

[22] At 1200 UTC, the Mistral was well established over the GoL as seen in Figures 5c, 6c and 7c: it maintained its cold and dry jet-like characteristics over a large portion of the GoL. The classical foehn type flow characteristics (i.e., warming and drying) were observed in the lee of the Pyrénées, the Massif Central, and Maritime Alps. Here also, the Mistral was observed to be colder and drier than the Tramontane.

[23] At 1500 UTC, a region of wind speeds less than 10 m s^{-1} was observed in the eastern part of the domain, which corresponds to the sheltering region (associated with

21562202c, 2003, C2, Downloaded from https://agupubs.onlinelibrary.wiley.com/doi/10.1029/2001JC001040 by Cochrane France, Wiley Online Library on [05/06/2023]. See the Terms and Conditions (https://onlinelibrary.wiley.com/terms-and-conditions) on Wiley Online Library for rules of use; OA articles are governed by the applicable Creative Commons License

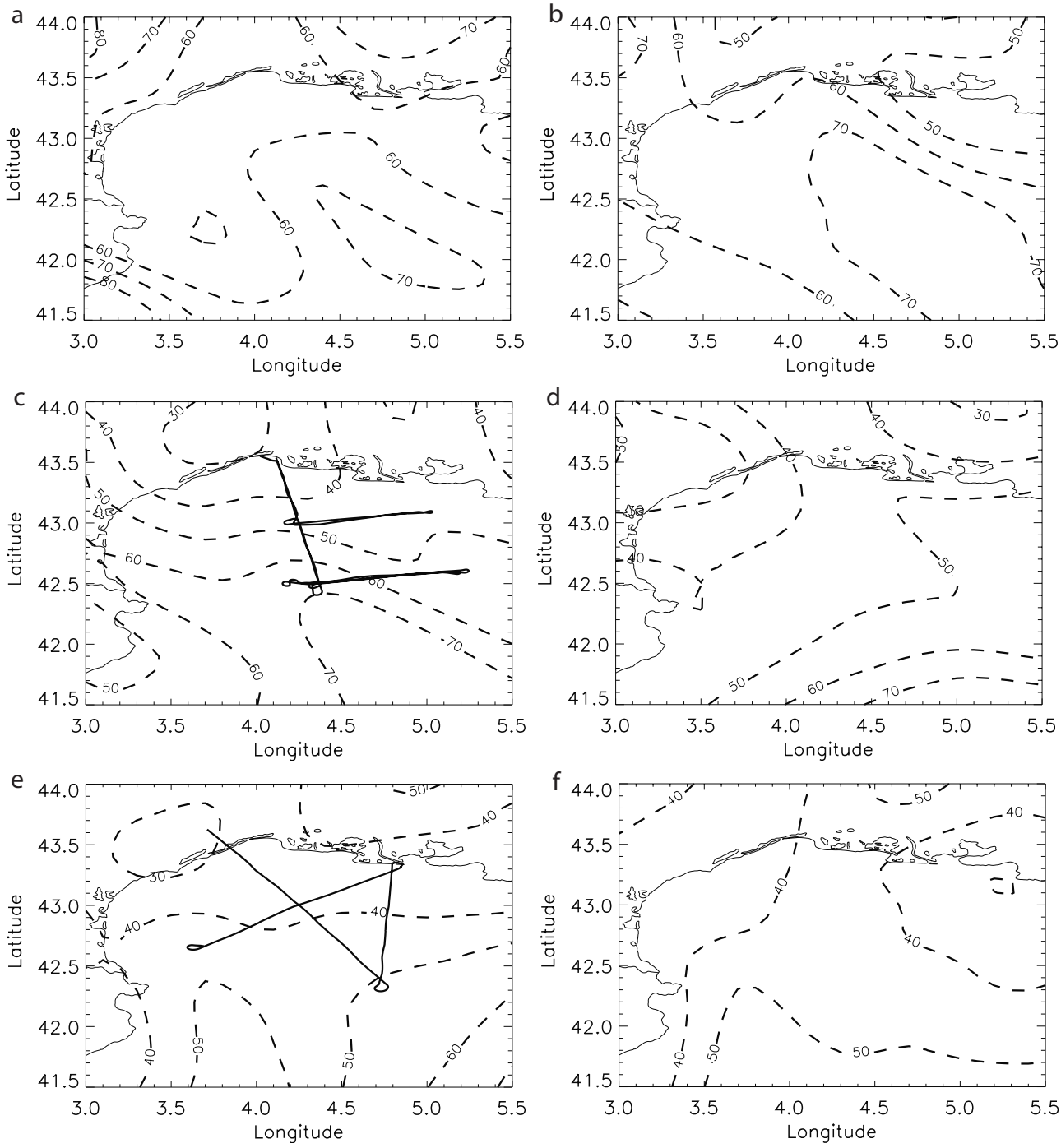

Figure 7. Relative humidity fields forecasted in the ABL (at 950 hPa) on 24 March 1998 by the French operational model ALADIN at (a) 0600, (b) 0900, (c) 1200, (d) 1500, (e) 1800, and (f) 2100 UTC. Superimposed are iso-RH between 0 and 100%, with 10% increments. Also superimposed are the ARAT trajectories in the morning (1200 UTC fields) and in the afternoon (1800 UTC fields).

the Maritime Alps) separating the Mistral from the outflow from the Gulf of Genoa (Figure 5d). As a result, the Mistral appeared to lose its characteristics over the Sea, the strongest winds associated with the mistral now being observed over the continent, in the Rhone Valley. In the mean time, the Tramontane flow did not seem to be affected by the outflow from the Ligurian Sea as both its location and strength remained relatively unchanged. In the northern GoL, the temperatures were again zonally distributed (Figure 6d). The temperature distribution over the sourthern GoL was influenced by the strong heating generated in the lee of the Pyrénées. The heating in the lee of the Massif central was also observed to be stronger than at 1200 UTC. Finally, the MABL air over the northwestern GoL was drier than previously, also due to the intensification of the foehn effect (Figure 7d). Nevertheless relative humidity (RH) values as high as 70% were observed in the southeastern part of the domain. Such

21562202c, 2003, C2, Downloaded from https://agupubs.onlinelibrary.wiley.com/doi/10.1029/2001JC001040 by Cochrane France, Wiley Online Library on [05/06/2023]. See the Terms and Conditions (https://onlinelibrary.wiley.com/terms-and-conditions) on Wiley Online Library for rules of use; OA articles are governed by the applicable Creative Commons License

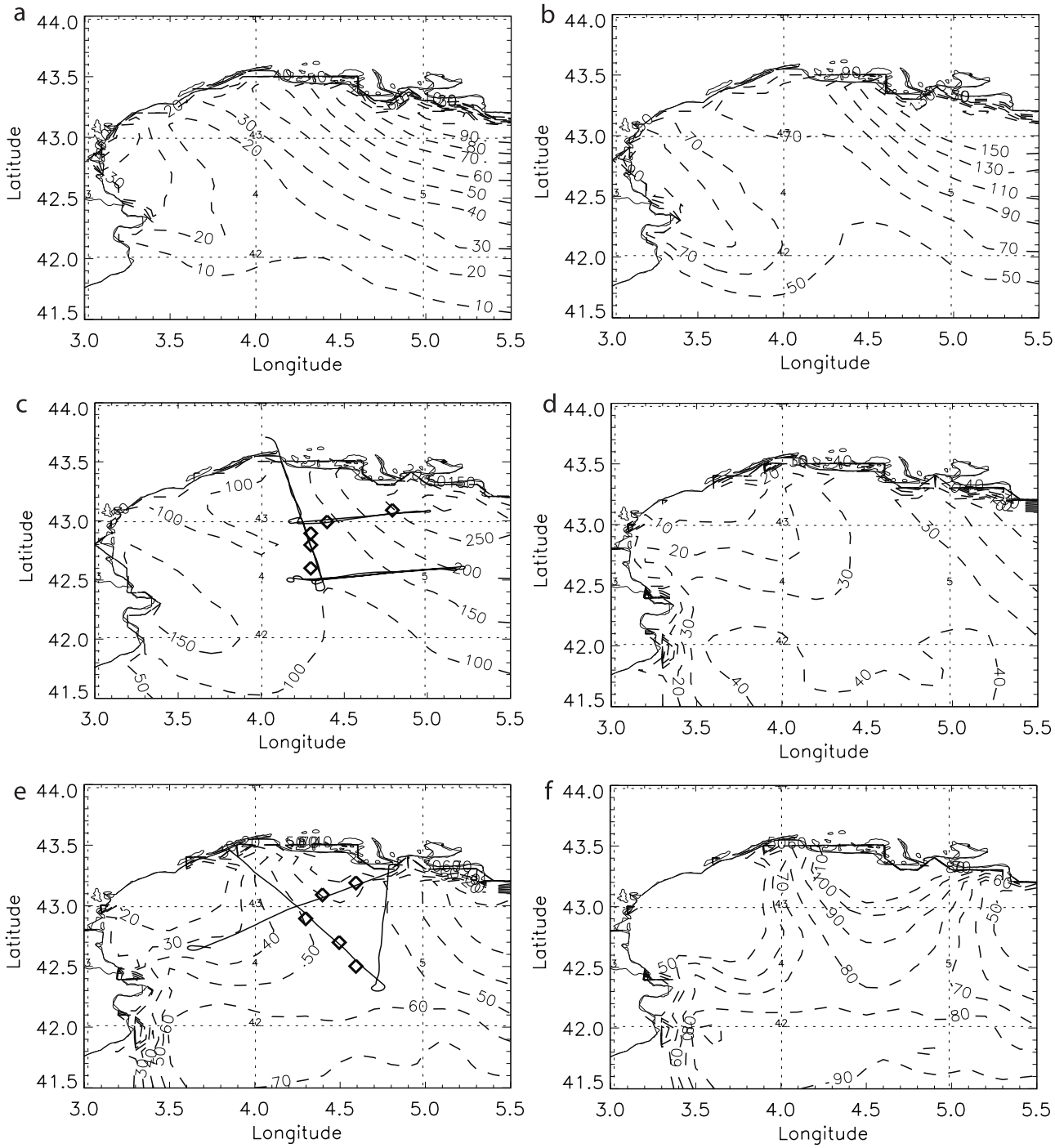

Figure 8. Surface sensible heat fluxes over the Mediterranean forecasted on 24 March 1998 by the French operational forecast model ALADIN at (a) 0600, (b) 0900, (c) 1200, (d) 1500, (e) 1800, and (f) 2100 UTC. Units are W m^{-2}. Superimposed are the ARAT tracks during F02 and F03 (solid lines). Diamonds indicate the positions where averaged turbulent heat fluxes were computed at the lowest level flown by the aircraft.

large RHs could correspond to moisture advected westward from the Tyrrhenian Sea cyclone as discussed below.

[24] At 1800 UTC, the Tramontane flow was observed to be shifted to the southwest as the Mistral began to intensify again. The influence of the sheltered region to the east of the Mistral also appeared to weaken. The sheltered region sperating the Mistral and the Tramontane was very narrow at that time (Figure 5e). The cold and jet-like characteristics of the Mistral were only maintained over the continent (Figure 6e). The warming and drying in the lee of the Massif Central at 1500 and 1800 UTC were comparable. The influence of the Alpine lee cyclone in terms of RH was still observable in the southeastern part of the domain (Figure 7e). In the northwestern part of the GoL, RHs were on the order of 40%.

[25] Finally at 2100 UTC, the Mistral flow was well established again. It had a more marked northerly direction than at 1200 UTC due to the southward displacement of the

21562202c, 2003, C2, Downloaded from https://agupubs.onlinelibrary.wiley.com/doi/10.1029/2001JC001040 by Cochrane France, Wiley Online Library on [05/06/2023]. See the Terms and Conditions (https://onlinelibrary.wiley.com/terms-and-conditions) on Wiley Online Library for rules of use; OA articles are governed by the applicable Creative Commons License

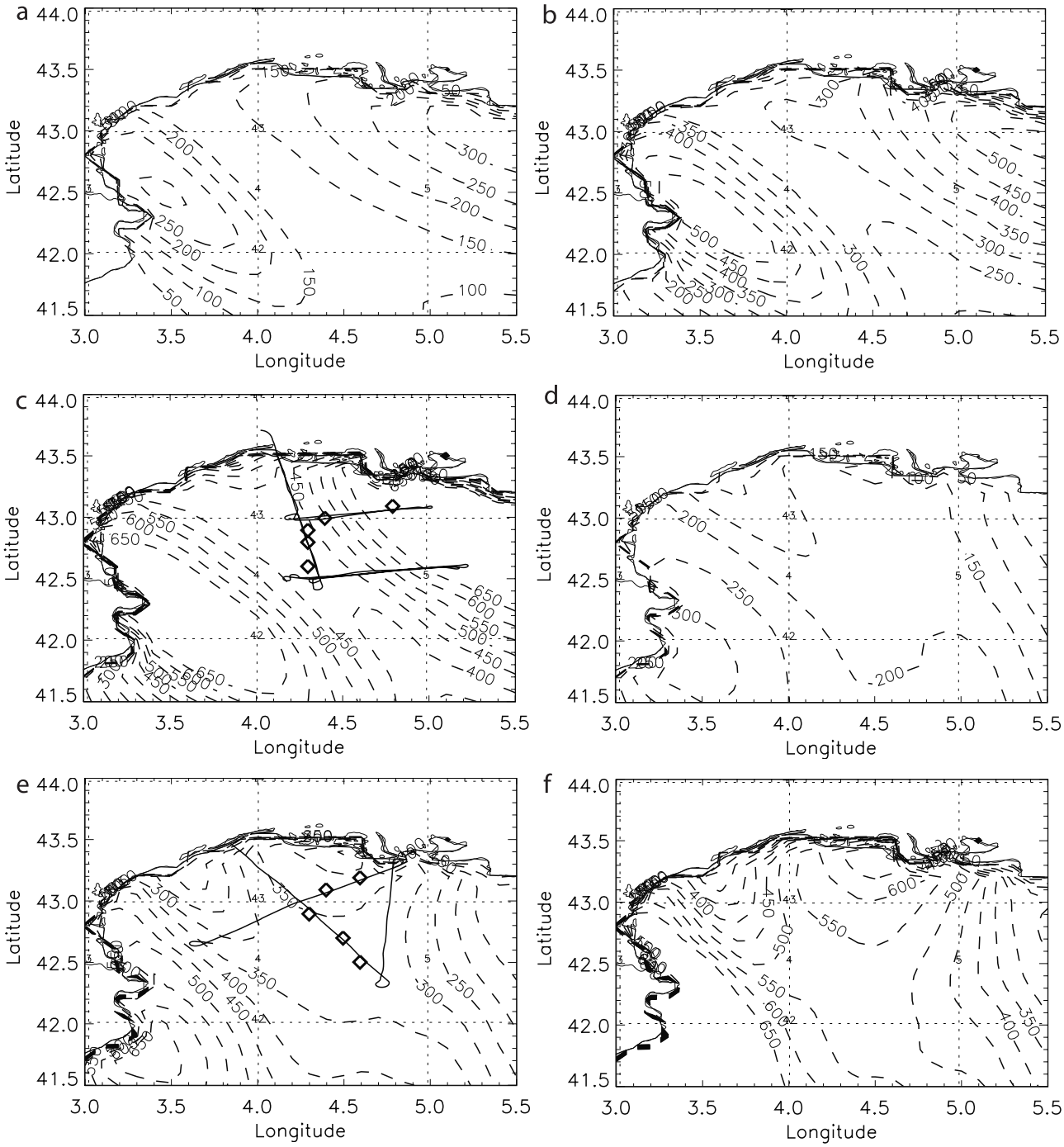

Figure 9. Surface latent heat fluxes over the Mediterranean forecasted on 24 March 1998 by the French operational forecast model ALADIN at (a) 0600, (b) 0900, (c) 1200, (d) 1500, (e) 1800, and (f) 2100 UTC. Units are W m^{-2}. Superimposed are the ARAT tracks during F02 and F03 (solid lines). Diamonds indicate the positions where averaged turbulent heat fluxes were computed at the lowest level flown by the aircraft.

Alpine lee cyclone (Figure 5f). The cold and dry characteristics of the Mistral were again well marked (Figures 6f and 7f, respectively). A strong foehn was observed in the lee of the Alps, in the eastern part of the domain.

[26] Among variables controlling the structure of the ABL, and hence the air-sea exchanges, cloudiness at the ABL top can play an important role. The cloud cover over the GoL at 1100 and 1600 UTC (at the time of F02 and F03, respectively) obtained from Meteosat visible images (not shown) evidences that aircraft measurements were made in clear air conditions, with the exception of the small cloud patch observed near way point D during F02.

5.2. Surface Turbulent Fluxes

[27] Not surprisingly, the sea surface temperature simulated by ALADIN did not evolve much during the day

21562202c, 2003, C2, Downloaded from https://agupubs.onlinelibrary.wiley.com/doi/10.1029/2001JC001040 by Cochrane France, Wiley Online Library on [05/06/2023]. See the Terms and Conditions (https://onlinelibrary.wiley.com/terms-and-conditions) on Wiley Online Library for rules of use; OA articles are governed by the applicable Creative Commons License

Table 1. Average Height of the Geopotential Associated With Constant Pressure Surfaces of the ALADIN Forecasts at 1200 and 1800 UTC in the FETCH Domain

Time	1000 hPa	950 hPa	925 hPa	900 hPa	850 hPa	800 hPa	700 hPa	600 hPa
1200 UTC	163 m	584 m	801 m	1022 m	1478 m	1956 m	2995 m	4172 m
1800 UTC	186 m	609 m	826 m	1049 m	1507 m	1987 m	3022 m	4186 m

(not shown, see section 3). On the contrary, surface sensible heat fluxes (SHFs) and surface latent heat fluxes (LHFs) computed with ALADIN between 0600 and 2100 UTC (Figures 8 and 9, respectively) exhibited an important spatiotemporal variability. The LHF field (Figure 9) exhibited regions characterized by large values (450 W m^{-2} and higher) associated with the established Tramontane and Mistral (e.g., at 0900, 1200 and 2100 UTC). In the earlier period, 0600 UTC, LHFs were weaker. However, patterns associated with the Mistral and Tramontane were recognizable. The effect of the sheltered region in the lee of the Massif Central was also clearly observed, in the form of a banner of reduced LHFs in between the Mistral and the Tramontane. This lee effect can extend as far as 250 km from the coast. The longest banners are generally observed to be associated with well-established, strong Tramontane/Mistral regimes.

[28] At the time when the cold air outbreak over the GoL was disrupted by the Ligurian Sea outflow (1500–1800 UTC), very weak LHFs were observed, most likely due to (i) weaker winds associated with the sheltered region in the lee of the Maritime Alps or/and (ii) westward advection of moisture from the Alpine lee cyclone. The Tramontane flow also appeared to be affected, as LHFs in that region were reduced by more than a factor of 2. In order to test the hypothesis about the influence of cyclone-related moisture advection, we have computed partial correlation coefficients of ALADIN LHF (at the lowest level of the model, i.e., 17 m) with the air-sea water vapor mixing ratio gradient, Δq, and the wind speed U over the GoL (Table 2). This was done for sea points only. The surface temperature field forecasted by ALADIN at 0000 UTC on 24 March 1998 has been used to define a land/sea mask which is then applied to temperature and moisture fields. The partial correlation coefficient between X and Y when the effects of Z is removed is [*Kendall and Stuart*, 1967]

$$r_{X,Y|Z} = \frac{r_{XY} - r_{XZ}r_{YZ}}{\sqrt{(1 - r_{XZ}^2)(1 - r_{YZ}^2)}}. \quad (1)$$

[29] Note that $r_{X,Y|Z} = r_{X,Y}$ if X and Y are uncorrelated. Hence, when computing the partial correlation coefficient between the LHF and U, we have removed the effect of humidity. Conversely, when computing the partial correlation coefficient between the LHF and Δq, we have removed the effect of wind speed.The air-sea water vapor mixing ratio gradient is computed as $\Delta q = q_s - q(z)$ where q_s is the water vapor mixing ratio at the surface computed for a temperature equal to the SST and assuming the surface relative humidity to be 100%, and $q(z)$ is the water vapor mixing ratio at altitude z. In Table 1 and Table 2, results are presented for q at 2 m ASL and at 1000 hPa. Similarly, partial correlation coefficients computed between LHFs and wind speed are presented for U at 10 m ASL and at 1000 hPa.

[30] Table 2 evidences that the so computed partial correlation coefficients does not depend on the altitude selected (i.e., 2/10 m or 1000 hPa). According to Table 2, during the first part of the day (i.e., 0600–1200 UTC), both Δq and U were significantly correlated with LHFs, even though correlation coefficients were sightly larger for U. In the second half of the day, LHF was significantly correlated with U only, the greatest correlation being obtained at 1500 UTC. Furthermore, during that period, LHF and Δq were anticorrelated. In conclusion, it appeared that during the time when the Alpine lee cyclone significantly disturbed the cold air outbreak over the GoL (1500–1800 UTC), air-sea moisture exchanges were mainly driven by dynamics.

[31] By comparison with the LHF field, the influence of the Mistral and Tramontane on the SHF field was only

Table 2. Partial Correlation Coefficient Between ALADIN Surface Sensible (Latent) Heat Flux (at 17 m ASL) and Air-Sea Temperature (Water Vapor Mixing Ratio) Difference Over the GoL on the FETCH Domain at 0600, 0900, 1200, 1500, 1800, and 2100 UTC on 24 March 1998[a]

	Sensible Heat Flux				Latent Heat Flux			
Time	2 m/10 m		1000 hPa		2 m/10 m		1000 hPa	
UTC	ΔT, C	U, m s^{-1}	ΔT, C	U, m s^{-1}	Δq, g kg^{-1}	U, m s^{-1}	Δq, g kg^{-1}	U, m s^{-1}
0600	0.67	0.17	0.71	0.10	0.46	0.64	0.49	0.56
0900	0.79	0.41	0.81	0.40	0.38	0.58	0.45	0.57
1200	0.66	0.44	0.61	0.40	0.41	0.73	0.46	0.74
1500	0.45	0.32	0.53	0.39	−0.03	0.90	−0.02	0.94
1800	0.62	0.38	0.59	0.42	−0.24	0.74	−0.16	0.77
2100	0.58	0.49	0.56	0.40	0.18	0.65	0.23	0.69

[a]Also given are the partial correlation coefficient between ALADIN surface heat fluxes and wind speed. Results are presented for atmospheric variables at 2 or 10 m ASL and at 1000 hPa. When computing the partial correlation coefficient between the LHF and U, we have removed the effect of humidity. Conversely, when computing the partial correlation coefficient between the LHF and Δq, we have removed the effect of wind speed.

215622022c, 2003, C2, Downloaded from https://agupubs.onlinelibrary.wiley.com/doi/10.1029/2001JC001040 by Cochrane France, Wiley Online Library on [05/06/2023]. See the Terms and Conditions (https://onlinelibrary.wiley.com/terms-and-conditions) on Wiley Online Library for rules of use; OA articles are governed by the applicable Creative Commons License

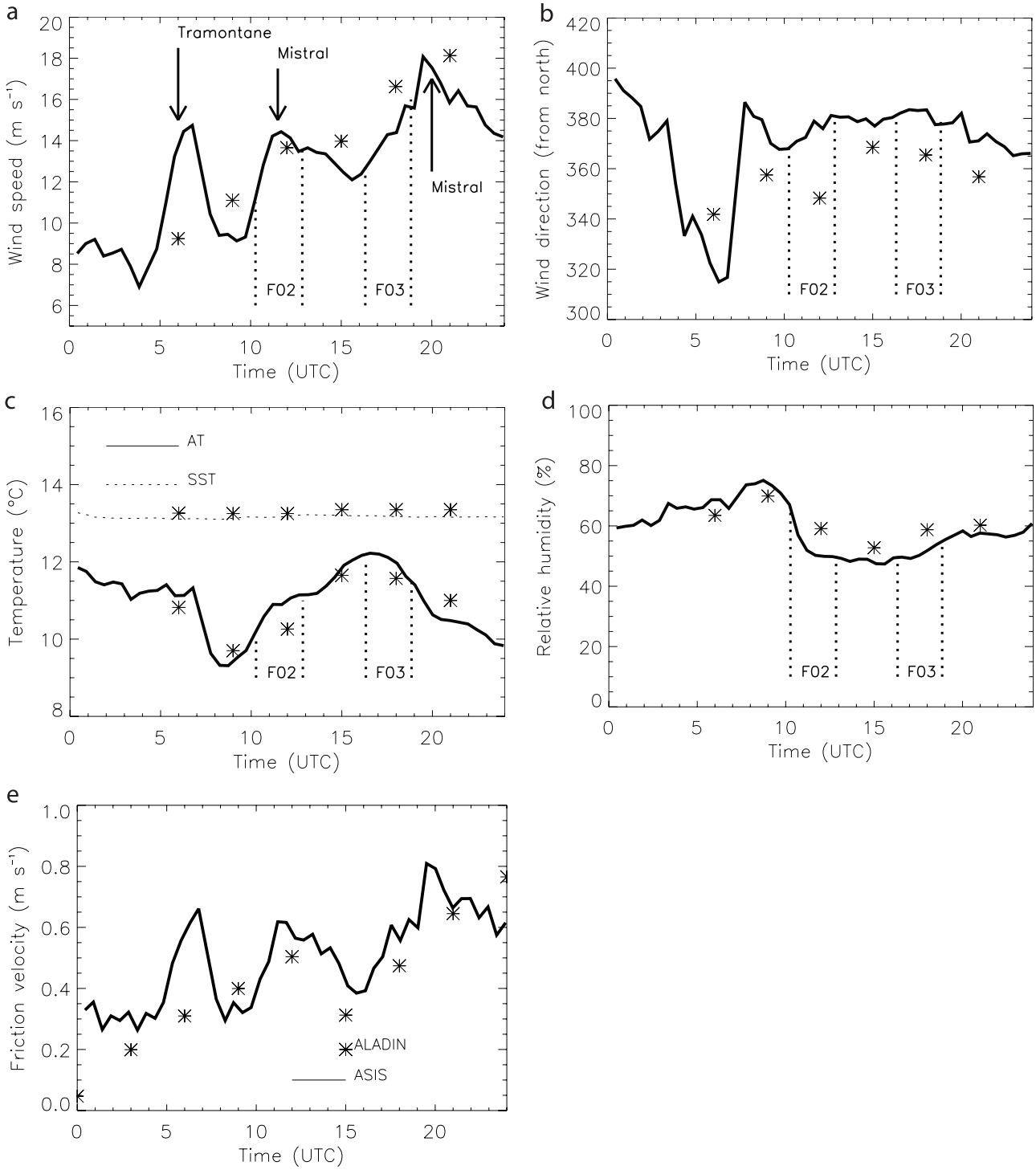

Figure 10. Diurnal evolution of the (a) wind speed, (b) wind direction, (c) air and sea temperature, (d) relative humidity, and (e) friction velocity measured by the ASIS buoy (solid line) and forecasted by ALADIN (asterix) on 24 March 1998. F02 and F03 indicate the time period during which airborne measurements were acquired in the morning and in the afternoon, respectively. Labels "Mistral" and "Tramontane" indicate the time periods at which these winds prevailed over the GoL.

evident during the first half of the day. However, during that period, the effect of the sheltered region in the lee of the Massif Central was not clearly observed. Distinct banners of reduced SHF could only be identified during the second half of the day. The analysis based on partial correlation coefficients also evidenced an essential difference between LHFs and SHFs: SHFs exhibited larger correlations with ΔT than with U, whereas LHFs exhibited larger correlations with U than with Δq. During the time when the Alpine lee cyclone significantly disturbed the cold air outbreak over

21562202c, 2003, C2, Downloaded from https://agupubs.onlinelibrary.wiley.com/doi/10.1029/2001JC001040 by Cochrane France, Wiley Online Library on [05/06/2023]. See the Terms and Conditions (https://onlinelibrary.wiley.com/terms-and-conditions) on Wiley Online Library for rules of use; OA articles are governed by the applicable Creative Commons License

the GoL, air-sea temperature exchanges were driven by both dynamics and temperature stratification.

6. Multiplatform Surface Turbulent Flux Measurements and Their Interpretation in the Meteorological Mesoscale Context

[32] As shown in the previous Section, the meteorological situation over the GoL was very unstationary on 24 March 1998. This resulted in a great spatiotemporal variability in terms of air-sea exchanges. The purpose of this section is to interpret time series of turbulent flux measurements in the light of the meteorological context. The quality of the turbulent flux measurements provided by ALADIN is discussed in-depth by *Eymard et al.* [2003].

6.1. Local Scale Analysis: ASIS Buoy Measurements

[33] In Figure 10, we compare the diurnal evolution of the wind speed and direction, sea surface and air temperature, RH and friction velocity measured at 7 m ASL by the ASIS buoy with their counterparts forecasted by ALADIN at 10 m ASL (wind) and 2 m ASL (temperature and RH), i.e., extracted at the location of the buoy. The wind measurements (Figures 10a and 10b) confirmed the nonstationary nature of the flow over the GoL. The three periods of established Tramontane (peaking at 0600 UTC, winds from the 320–340°) and Mistral (peaking at 1200 and 2000 UTC, winds from the 0–20°) are evidenced. These events were separated by periods during which the wind speeds were reduced. In terms of dynamics, ALADIN predicted continuously strengthening winds between 0600 and 2100 UTC. Furthermore, ALADIN completely missed the wind speed maximum associated with the Tramontane. As shown in Figure 4 (and Figure 5), the Tramontane event was forecasted by ALADIN. However, according to the ASIS measurements, the core of the Tramontane jet was not forecasted in the right location, but too far south. This is corroborated by Figure 10b which shows that the wind direction forecasted by ALADIN at the location of ASIS had a marked northerly component (340°) when ASIS measurements indicated a more zonal flow (315°). After 0900 UTC, the wind speeds associated with the Mistral simulated with ALADIN were slightly overestimated (except at 1200 UTC). During the same period, ASIS measurements evidenced the Mistral to have a small easterly component which was reproduced by ALADIN only at 1500 and 1800 UTC. Besides, ALADIN did not handle properly the transition phases between the different regimes (i.e., at 0900 and 1500 UTC), during which the wind speed is generally overestimated. Not surprising, the same imperfections also occurred on the simulated friction velocity (Figure 10e). Nevertheless, ALADIN did a better job of capturing the transition between the 2 Mistral events (reduced friction velocity was indeed observed). Even though slightly underestimated, friction velocities computed with ALADIN were of the same order of magnitude as those measured by ASIS. On the other hand, ALADIN-derived RH and air temperature (at 2 m ASL) as well as sea surface temperature were found in remarkable agreement with ASIS measurements. As discussed in the Appendix, this was not necessarily the case in the ABL.

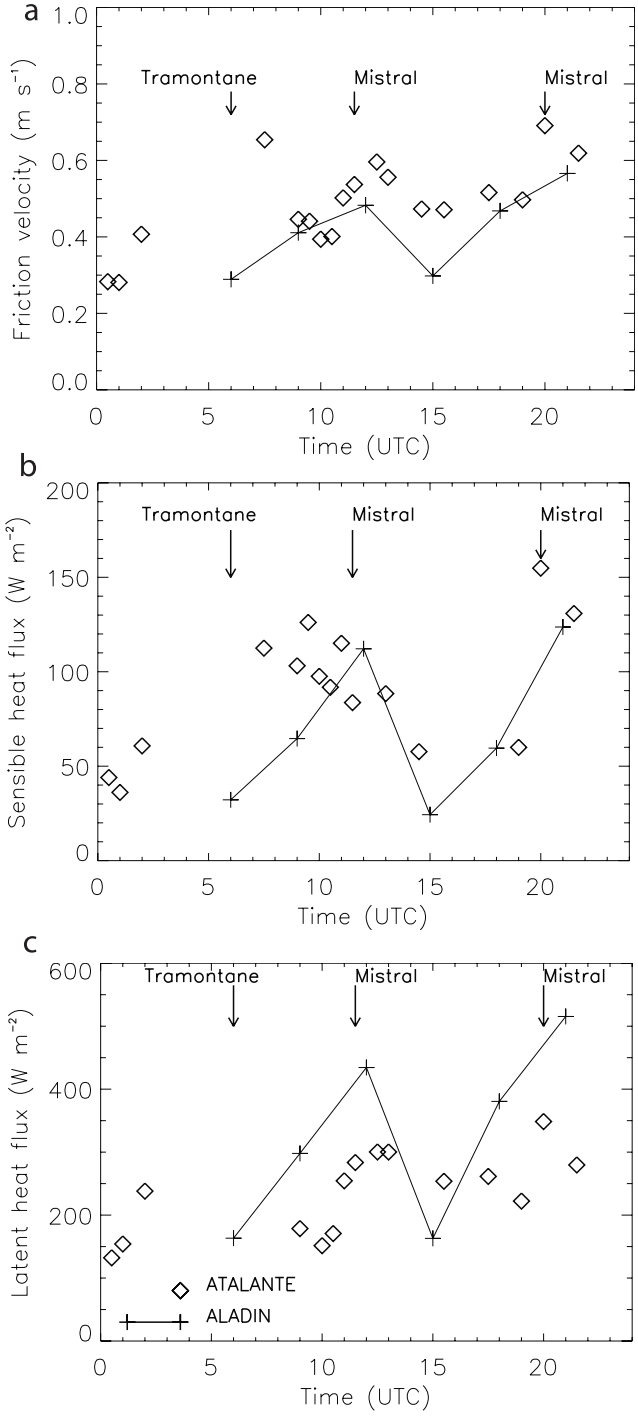

Figure 11. Diurnal evolution of the (a) friction velocity, (b) surface sensible heat flux, and (c) surface latent heat flux on 24 March 1998 as measured from the R/V *Atalante* (diamonds) (using a dissipative technique) and forecasted by ALADIN (crosses). Labels "Mistral" and "Tramontane" indicate the time periods at which the Mistral and Tramontane regime where prevailing over the GoL.

[34] Despite not being very accurate, ALADIN forecasts can be used to interpret the origin of the wind speed gaps observed by ASIS at 0900 and 1600 UTC. According to Figures 5a–5c, the former gap was caused by the southward

215622022c, 2003, C2, Downloaded from https://agupubs.onlinelibrary.wiley.com/doi/10.1029/2001JC001040 by Cochrane France, Wiley Online Library on [05/06/2023]. See the Terms and Conditions (https://onlinelibrary.wiley.com/terms-and-conditions) on Wiley Online Library for rules of use; OA articles are governed by the applicable Creative Commons License

Table 3. Friction Velocity (u_*) and Surface Latent and Sensible Heat Fluxes (Q_s and Q_l, Respectively) Measured on Board Aircraft (a/c) Using an Eddy Correlation Technique (the Merlin IV (Morning) and the ARAT (Afternoon)) on 24 March 1998[a]

	Position		Time, UTC		Altitude, m ASL		u_*, m s^{-1}		Q_s, W m^{-2}		Q_l, W m^{-2}	
	Lat	Lon	a/c	Model	a/c	Model	a/c	Model	a/c	Model	a/c	Model
	42.6	4.3	1123	1200	95	17	0.52	0.28	45	102	202	418
Established	42.8	4.3	1128	1200	97	17	0.45	0.26	36	109	156	429
	42.9	4.3	1132	1200	99	17	0.35	0.25	29	119	195	450
Mistral	43.0	4.4	1139	1200	99	17	0.63	0.25	56	119	333	450
	43.1	4.8	1144	1200	92	17	0.65	0.57	93	250	393	736
	42.5	4.6	1754	1800	109	17	0.53	0.20	44	54	267	332
Disrupted	42.7	4.5	1800	1800	113	17	0.44	0.22	25	54	181	345
	42.9	4.3	1806	1800	117	17	0.43	0.22	18	52	198	355
Mistral	43.1	4.4	1814	1800	122	17	0.56	0.23	33	55	283	365
	43.2	4.6	1820	1800	112	17	0.78	0.26	66	71	380	408

[a]These measurements are compared to the variables extracted from the ALADIN forecasts at 1200 and 1800 UTC, respectively, at the location of the aircraft measurements.

drift of the sheltered region as the wind regime over the GoL shifted from a Tramontane regime to a Mistral regime. Between 0700 and 1200 UTC, the ASIS buoy was alternatively located south of, in and north of the sheltered region. The latter gap in wind speed caused by the meandering of the sheltered region in the lee of the Maritime Alps (Figure 5c–e). This sheltered region was pushed westward (toward the ASIS buoy) as the depression deepened between 1200 and 1600 UTC, thereby influencing the ASIS measurements. After 1600 UTC, as the influence of the Ligurian Sea outflow was weakening, the sheltered region in the lee of the Maritime Alps drifted back eastward (Figure 3), causing the increase in wind speed observed in the ASIS data.

6.2. Mesoscale Analysis: Aircraft and Ship Measurements

[35] In Figure 11, we compare the diurnal evolution of the friction velocity, LHF and SHF estimated from measurements made at 17 m ASL on board the R/V *Atalante* (H. Dupuis et al., Impact of flow distortion corrections on turbulent fluxes estimated by the inertial-dissipation method during FETCH experiment on R/V *Atalante*, submitted to *Journal of Geophysical Research*, 2002, hereinafter referred to as Dupuis et al., submitted manuscript, 2002) with their counterparts forecasted by ALADIN at approximately the same level, i.e., extracted along the trajectory of the *Atalante* on 24 March 1998 (Figure 2c). Surface turbulent fluxes are calculated using an inertial dissipation method [*Dupuis et al.*, 1997; Dupuis et al., submitted manuscript, 2002]. Not surprisingly, here also, ALADIN misses the Tramontane event (the ship was located to the east of the ASIS buoy). Nevertheless, it captured the 2 heat flux maxima associated with the established Mistral regime. Here also, the wind speed decrease between 1200 and 2100 UTC is caused by the meandering of the sheltered region in the lee of the Maritime Alps. ALADIN overestimated (underestimated) LHFs during periods of stronger (weaker) wind. Reasons for this have been investigated by *Eymard et al.* [2003] and are related to the turbulent flux parameterization in the model (ALADIN fluxes are integrated over a 3 hour period, the exchange coefficients used in the bulk parametrization of fluxes increase with wind speed) as well as several shortcomings of the model (ALADIN underestimates the RH in the ABL, the SST in the model is biased by 0.5–1°C). By comparison, the evolution of SHFs was better described by ALADIN. In all cases, turbulent fluxes computed with ALADIN were of the same order of magnitude as those measured on board the ship.

[36] Finally, airborne turbulent flux measured on board the Merlin (morning, around 1100 UTC) and the ARAT (afternoon, around 1800 UTC) using an eddy correlation technique are presented in Table 3. These measurements were obtained from data on 25–30 km long levelled legs. The position of the center of each leg is shown in Figure 8. The average altitude at which these measurement were made ranged between 92 and 122 m ASL. The accuracy of the measurements at these heights ranges between 10 and 20% for LHFs and SHFs, while the accuracy on the friction velocity is of the order of 30% [*Lambert and Durand*, 1998]. Systematic error associated with these measurements is less than 10%. Measurements are representative of heat exchanges over a fairly limited area (see Figure 8, for example). Nevertheless, a great spatial variability was observed as in the ALADIN fields. In the morning, large LHFs (>300 W m^{-2} at 100 m ASL) were associated with the Mistral and weaker values (200 W m^{-2} or less) were measured in the sheltered area. A similar behavior is observed for SHFs. In the afternoon model predicted SHF are weaker by a factor of 2 while measured SHF are reduced about 30% compared to the morning values. LHFs were observed to be slightly weaker than in the morning. However, most of the measurements at that time were made in a region near the coast where the influence of the Mistral could be felt. More importantly, the fluctuations of SHF and LHF along the aircraft tracks are consistent with the mesoscale picture provided by ALADIN. We did not attempt a systematic comparison between measured and modelled turbulent fluxes, because airborne measurements where made too high.

7. Influence of Alpine Lee Cyclogenesis on the Vertical Structure of the Flow Over the Gulf of Lion

[37] The structure of the flow and its evolution with time has been analyzed using in situ aircraft and balloon soundings, as well as high resolution measurements of tropospheric water vapor mixing ratio and atmospheric reflectivity, made by the airborne lidar LEANDRE 2 [*Bruneau et al.*, 2001a, 2001b]. Because it is sensitive to relative humidity as well as aerosol properties and concentration, lidar-derived reflectivity is extremely useful to investigate ABL structural properties [e.g., *Flamant and Pelon*, 1996; *Flamant et al.*, 2000]. Here we only discuss reflectivity

215622022c, 2003, C2, Downloaded from https://agupubs.onlinelibrary.wiley.com/doi/10.1029/2001JC001040 by Cochrane France, Wiley Online Library on [05/06/2023]. See the Terms and Conditions (https://onlinelibrary.wiley.com/terms-and-conditions) on Wiley Online Library for rules of use; OA articles are governed by the applicable Creative Commons License

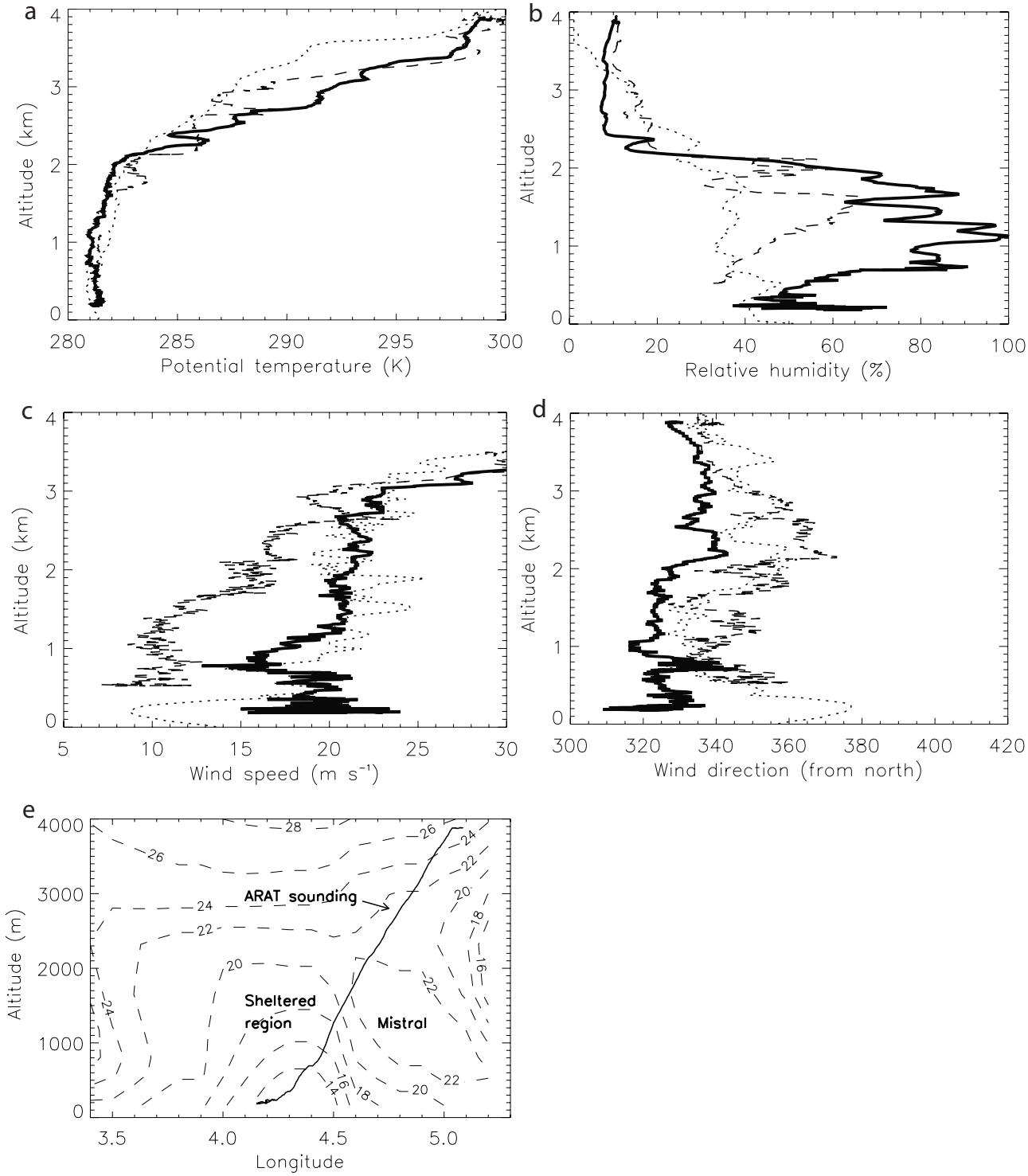

Figure 12. Profiles of (a) potential temperature, (b) relative humidity, (c) wind speed, and (d) wind direction obtained during the ascent (i.e., coastal region - dashed line) and descent (i.e., open GoL - solid line) soundings of the ARAT during F02. The dotted line is obtained from the balloon sounding launched from the *Atalante* at 1200 UTC. (e) The route and heights of the descent sounding performed over the GoL are superimposed on a 2D vertical cross section of wind speed forecasted by ALADIN in a plane containing way points E and D.

measurements which vertical and horizontal resolutions are 160 and 15 m, respectively. The water vapor mixing ratio measurements are presented and discussed in a companion paper [*Flamant et al.*, 2003].

7.1. Representativity of Aircraft Soundings

[38] According to Figures 5c and 5e, the aircraft sounding performed during the ascent, between the city of Montpellier airport and way point A, of F02 and F03 were

215622022c, 2003, C2, Downloaded from https://agupubs.onlinelibrary.wiley.com/doi/10.1029/2001JC001040 by Cochrane France, Wiley Online Library on [05/06/2023]. See the Terms and Conditions (https://onlinelibrary.wiley.com/terms-and-conditions) on Wiley Online Library for rules of use; OA articles are governed by the applicable Creative Commons License

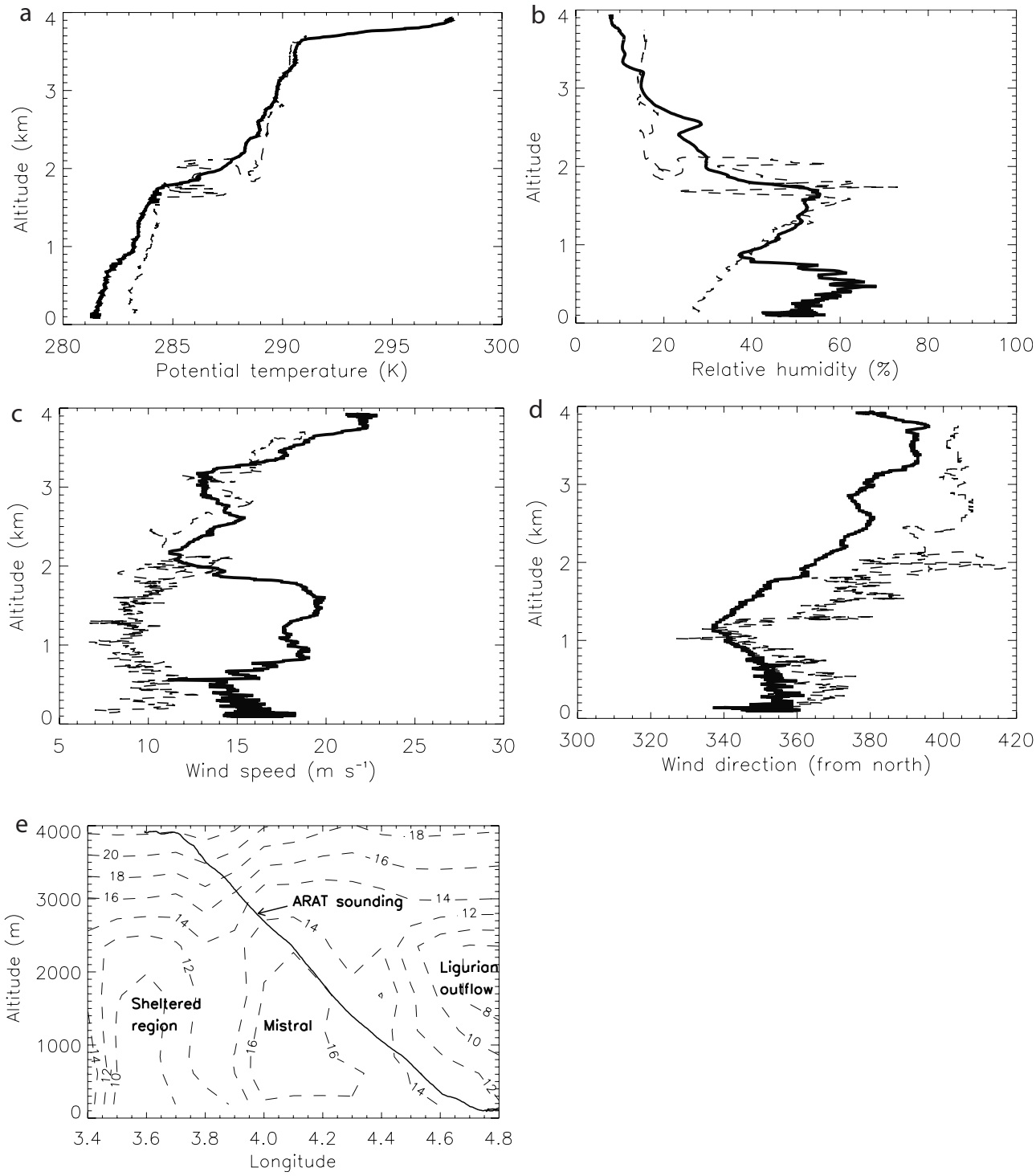

Figure 13. Profiles of (a) potential temperature, (b) relative humidity, (c) wind speed, and (d) wind direction obtained during the ascent (coastal region - dashed line) and descent (open GoL - solid line) soundings of the ARAT during F03. (e) The route and heights of the descent sounding performed over the GoL are superimposed on a 2D vertical cross section of wind speed forecasted by ALADIN in a plane containing way points E and F.

representative of the thermodynamics in the vicinity of the western edge of the Mistral (i.e., close to the sheltered region).

[39] The sounding performed during the descent between D and E of F02 (Figure 12) documented the thermodynamics across the eastern edge of the sheltered region: below 0.7 km ASL, the measurements are representative of the conditions prevailing in the sheltered region at the western edge of the Mistral, while above 1 km ASL, the measurements are representative of the conditions above the Mistral flow

21562202c, 2003, C2, Downloaded from https://agupubs.onlinelibrary.wiley.com/doi/10.1029/2001JC001040 by Cochrane France, Wiley Online Library on [05/06/2023]. See the Terms and Conditions (https://onlinelibrary.wiley.com/terms-and-conditions) on Wiley Online Library for rules of use; OA articles are governed by the applicable Creative Commons License

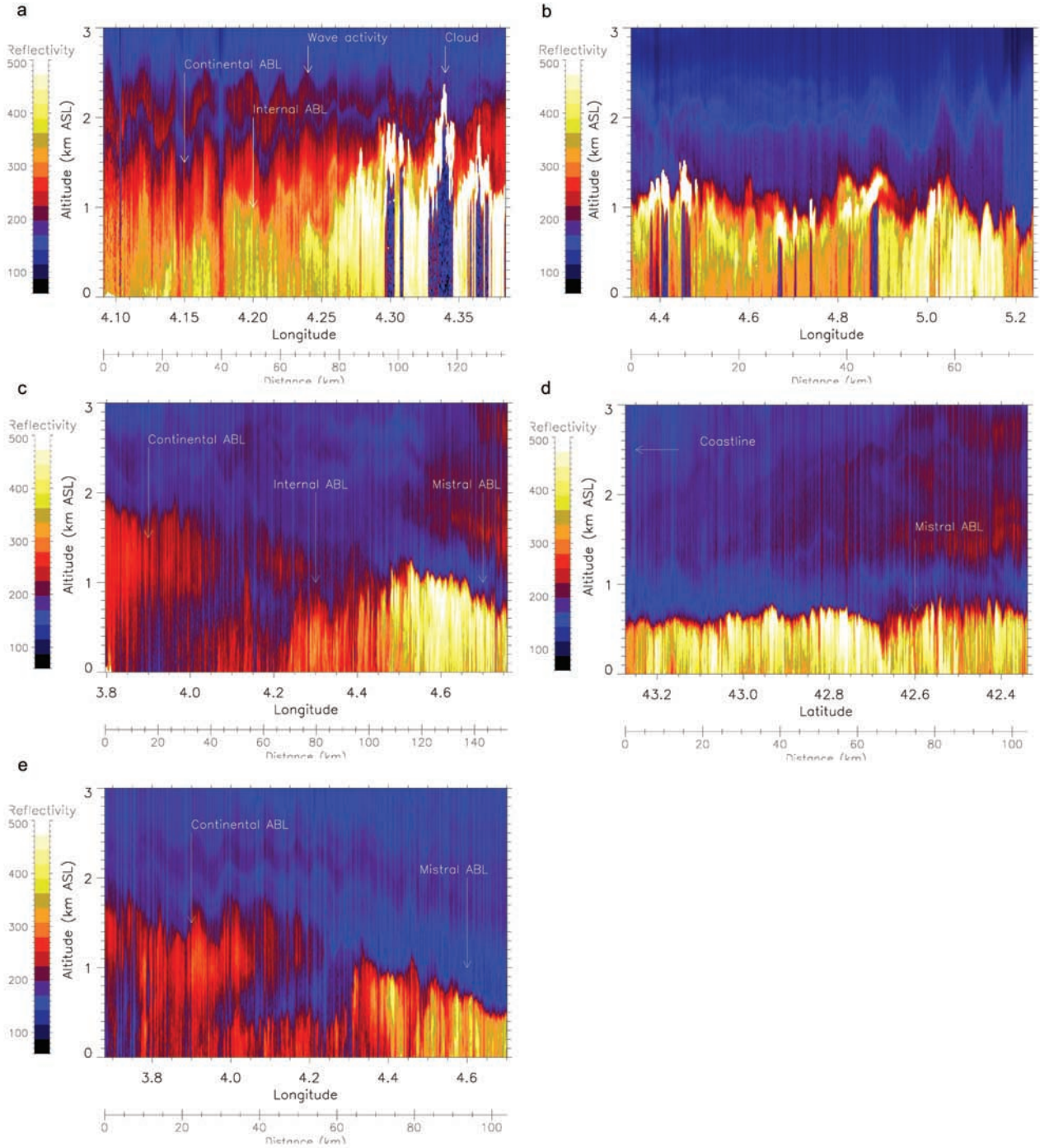

Figure 14. Atmospheric reflectivity at 0.73 μm as obtained from LEANDRE 2 along (a) leg AD and (b) leg DE of the morning flight and along (c) leg AF, (d) leg FC, and (e) leg CE of the afternoon flight. Way points A and D are to the left of Figures 14a and 14b, respectively. Way points A, C, and E are to the left of Figures 14c, 14d, and 14e, respectively.

(Figure 12e). Note that, at 1200 UTC (time of the balloon launch), the Atalante was also positioned along the western edge of the Mistral (eastern edge of the sheltered region). The sounding performed during the descent between E and F of F03 (Figure 13) documented the thermodynamics across the southernmost extend of the disrupted Mistral. Between 1.5 and 3 km, the aircraft sounding performed over the GoL was representative of the dynamics in the Mistral flow, while below 1 km ASL, the sounding was representative of the dynamics in the eastern edge of the Mistral perturbed by the outflow from the Ligurian sea connected with the depression (Figure 13e).

21562202c, 2003, C2, Downloaded from https://agupubs.onlinelibrary.wiley.com/doi/10.1029/2001JC001040 by Cochrane France, Wiley Online Library on [05/06/2023]. See the Terms and Conditions (https://onlinelibrary.wiley.com/terms-and-conditions) on Wiley Online Library for rules of use; OA articles are governed by the applicable Creative Commons License

7.2. Atmospheric Boundary Layer Structure and Related Dynamics in the Well-Established Mistral

[40] Figure 12 shows that the vertical structure of the Mistral flow in the late morning (at the time when the Mistral flow was well established) did not evolve much between the coast and way point E as the temperature profiles obtained from aircraft and balloon were very similar. The jet-like structure of the Mistral was observed in the lower part of both soundings, near the coast and in the vicinity of way point E (Figure 12c). In both cases, the flow was rather dry in the ABL (Figure 12a) and the wind speed was minimum just above the ABL. Above the Mistral, winds in the continental ABL were observed to be relatively constant in magnitude ($\approx$20 m s^{-1}) and in direction (from 325–335°). The flow was also observed to be moist. Near the coast, on the edge of the sheltered region, the wind was from 345° (on average) and on the order of $\approx$10 m s^{-1} in the continental ABL. Close to the coast, we observed a rather well-mixed layer about 1.8 km deep, corresponding to the continental ABL advected over the sea (Figure 12a). In the vicinity of way point E, 2 temperature inversions were observed at 1.1 km and 2 km, the latter corresponding to the advected continental ABL, and the former corresponding top the marine ABL. Above the continental layer, wave activity was observed on all three soundings. All of these features were corroborated by lidar measurements as now discussed.

[41] The structure of the ABL was documented by lidar along legs AD and DE. According to Figure 5, leg AD was positioned inside and along the western edge of the sheltered zone (the western edge of the Mistral). Conversely, leg DE ran across the eastern edge of the sheltered region, way point E being located in the core of the Mistral. Along leg AD, an internal thermal boundary layer was observed to develop from the coast within the advected continental ABL as a result of the combined effect of roughness length reduction (at the land-sea transition) and enhanced surface turbulent fluxes related to the cold air advection over a warmer sea [e.g., *Flamant and Pelon*, 1996]. The top of the continental ABL was indeed observed around 2 km ASL on lidar measurements. The internal thermal boundary layer deepened with the distance to the coast, reaching a depth of 1.5 km near way point D. Large modulations of the ABL depth were observed to be associated with strong updrafts in the ABL and cloud formation (the low reflectivity values below the clouds are due to the extinction of the laser beam). Clouds as well as higher reflectivity values were observed near D, consistently with the large RH values forecasted at 1200 UTC by ALADIN (Figure 7c). Along leg DE, the averaged depth of the ABL was approximately 1 km. In the easternmost half of leg DE larger reflectivity values were consistent with higher RH forecasted by ALADIN (Figure 7).

[42] Along leg AD, the ABL top height fluctuated by $\approx$ $\pm$250 m around its average value. Simultaneously, wave-like features were also observed by lidar within the continental ABL. In Figure 15, we show the vertical velocity measured in situ simultaneously to the lidar measurements displayed in Figure 14a. This measurements evidenced that gravity waves were indeed present above the marine ABL. Also shown in Figure 15 is the evolution of the lidar reflectivity at the altitude of 2.4 km ASL along leg AD. The lidar-derived reflectivity series has been detrended and divided by 20 so to match the maximum amplitude of the vertical velocity fluctuations. Interestingly, lidar reflectivity was observed to be anticorrelated with vertical velocity (i.e., out of phase, shifted by π), except near way point D.

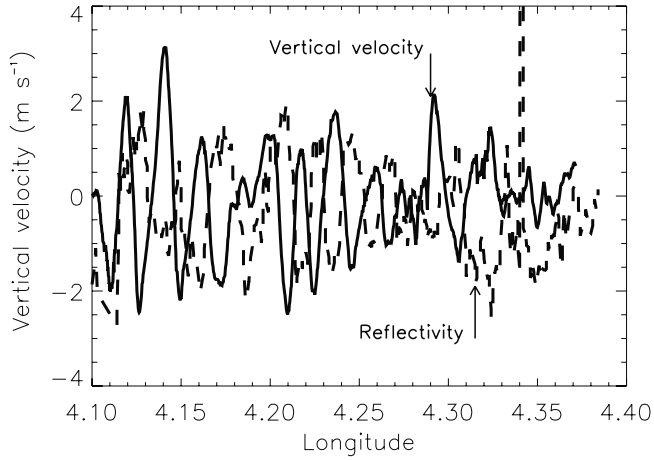

Figure 15. Vertical velocity measured in situ by the ARAT simultaneously to the lidar measurements displayed in Figure 14a during F02 on leg AD. Superimposed is the evolution of the lidar reflectivity at the altitude of 2.4 km ASL. The lidar-derived reflectivity series has been detrended and divided by 20 to match the maximum amplitude of the vertical velocity fluctuations.

7.3. Atmospheric Boundary Layer Structure and Related Dynamics in the Perturbed Mistral

[43] The potential temperature soundings near the coast and in the perturbed part of the Mistral evidenced a marked inversion at 1.7 km ASL coinciding with a RH maximum (Figure 13). Near way point F, a second inversion was present at 0.7 km ASL also corresponding to large RH values. These inversions corresponded to the continental and marine ABL, respectively. There was no evidence of wave activity. Close to the shoreline, the wind in the ABL presented the same jet-like structure than in the unperturbed case. This was no longer the case near way point F, where wind speed decreased with height in the marine ABL. Furthermore, the winds above the marine ABL in this region exhibited a marked northeasterly component in connection with the outflow coming from the Ligurian sea (not shown). Note that the outflow was much weaker at 1200 UTC.

[44] During F03, the structure of the ABL was documented by lidar along legs AF, FC and CE. According to Figure 5, legs AF and CE ran across the Mistral, way point A being located in the eastern edge of the sheltered region, way point F in the region to the east of the Mistral jet in which the wind speed decreases, and way point E being located in the sheltered region in the lee of the Massif Central. On leg FC, LEANDRE 2 sampled the ABL structure in a region of deceleration on the western edge of the Mistral. Lidar measurements on leg AF (Figure 14c) evidenced an internal thermal boundary layer developing from the coast (within the advected continental ABL) and reach a depth of 1200 m. The ABL depth fluctuations were not observed to be as important as in the morning. Coinci-

21562202c, 2003, C2, Downloaded from https://agupubs.onlinelibrary.wiley.com/doi/10.1029/2001JC001040 by Cochrane France, Wiley Online Library on [05/06/2023]. See the Terms and Conditions (https://onlinelibrary.wiley.com/terms-and-conditions) on Wiley Online Library for rules of use; OA articles are governed by the applicable Creative Commons License

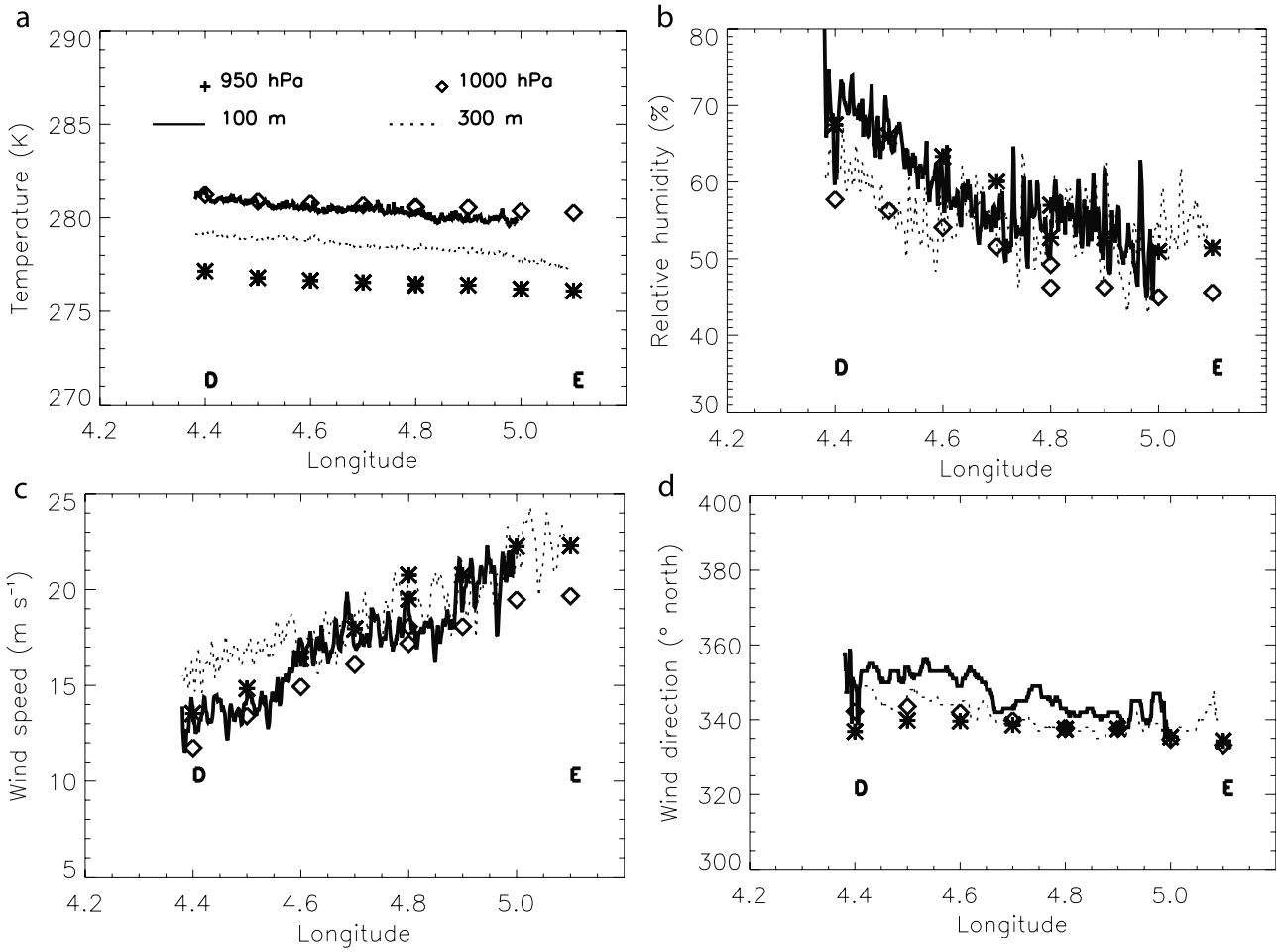

Figure A1. Comparison of (a) temperature, (b) relative humidity, (c) wind speed, and (d) wind direction extracted from the 1200 UTC ALADIN forecasts along leg DE at 1000 and 950 hPa (diamonds and asterisks, respectively) with measurements made in the ABL by the ARAT on the same leg at 100 and 300 m (solid and dashed lines, respectively).

dentally, gravity wave activity above the ABL was not observed. Thermals were not observed to be as energetic enough to significantly deform the temperature inversion at the ABL top and, hence, trigger condensation. This is consistent with the fact that the simulated and measured surface fluxes were smaller than in the morning.

[45] Close to way point F, at approximately 4.5°E, the marine ABL structure characteristics over the sea changed dramatically: it was observed to be shallower (700 m, Figure 14c) and was characterized by larger values of atmospheric reflectivity. This was confirmed by measurements made on leg FC (Figure 14d), along which the marine ABL was characterized by values of atmospheric reflectivity similar to those observed near way point F. Also, the marine ABL was observed to remain shallow (more so than in the established Mistral case), its depth gradually decreasing from 700 to 500 m with the distance to the coast. Furthermore, the large fluctuations of the ABL top observed in the established Mistral case are no longer observed. According to ALADIN forecasts, the collapse of the ABL is not due to diminishing LHF and/or SHF in that region (surface fluxes were forecasted to be nearly constant). The increase of lidar reflectivity observed east of 4.4°E over the GoL could be caused by (i) an increase in RH and/or (ii) an increase in aerosol concentration. The first hypothesis is not consistent with the 1800 UTC ALADIN RH field (Figure 7b) nor with aircraft in situ measurements of RH (see Appendix). Moreover, RH values were observed to be relatively low in the middle of the ABL (see Appendix) and the small fluctuations of RH (less than 10%) cannot alone account for the observed increase of reflectivity. Hence, the larger reflectivity in the eastern part of the sampled region are thought to be related to larger concentrations of pollution aerosol from the city of Marseille and the industrial petrochemical complex of Berre/Fos. Unfortunately, the highly spatially resolved aerosol measurements needed to (un)validate this hypothesis have not been made.

[46] On leg CE (Figure 14e), close to the coast, the ABL structure was similar to that observed along FC (i.e., shallow). The depth of the ABL increased westward from 500 to 1000 m (between 4.7 and 4.3°E) while reflectivity decreased significantly. Further to the west, a continental ABL was observed in the sheltered region in the lee of the Massif Central. In this region, lidar measurements evidence the presence of gravity waves inside the continental ABL.

215622022c, 2003, C2, Downloaded from https://agupubs.onlinelibrary.wiley.com/doi/10.1029/2001JC001040 by Cochrane France, Wiley Online Library on [05/06/2023]. See the Terms and Conditions (https://onlinelibrary.wiley.com/terms-and-conditions) on Wiley Online Library for rules of use; OA articles are governed by the applicable Creative Commons License

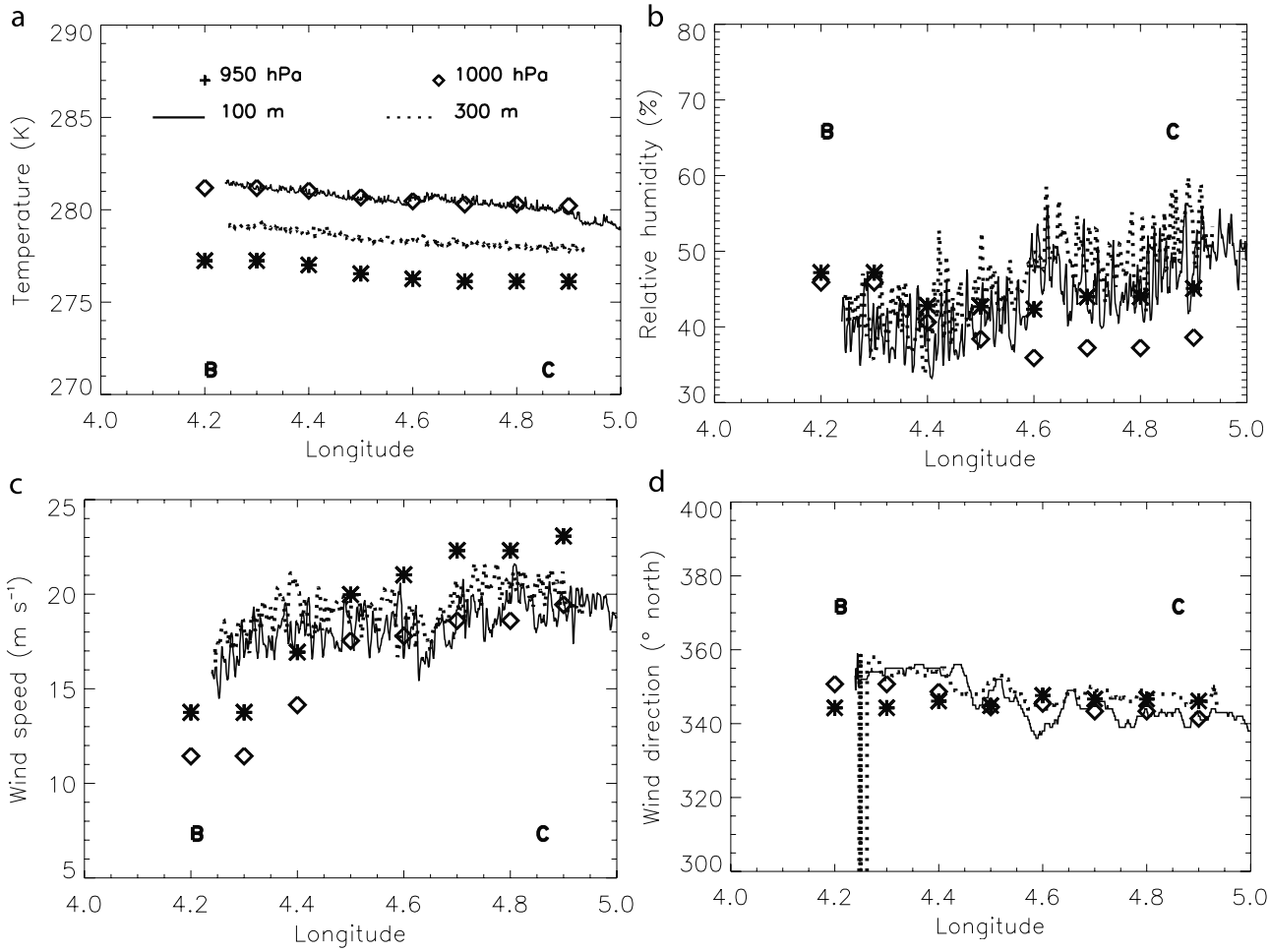

Figure A2. Same as Figure A1 but for leg BC.

[47] In the afternoon, the picture emerges that the influence of the outflow (which was more marked above than within the ABL) acted as a lid preventing the Mistral driven marine ABL from developing and thus preventing the possible occurrence of gravity waves (i.e., gravity waves triggered by the local deformation of the temperature inversion at the ABL top which in turn act as an obstacle to the flow in the free troposphere).

8. Summary and Conclusion

[48] In this paper, we have described the thermodynamics and the structure of the ABL over the GoL on 24 March 1998. We have evidenced that the depression located over the Tyrrhenian Sea had a significant influence on the strength and the direction of the Tramontane/Mistral flow over the GoL. It was shown that the Tramontane prevailed in the morning (0500–0800 UTC) prior to a period of established Mistral which peaked around 1200 UTC. In the afternoon, the Mistral was progressively disrupted by a strengthening outflow from the Ligurian Sea in connection with the deepening depression. These strong winds were appeared to be further accelerated by the presence of the Apennine range. In the evening (2000–2100 UTC), the Mistral was again well established over the GoL as the depression moved further south and the influence of outflow from the Ligurian Sea became weaker.

[49] The spatiotemporal variability of the LHFs and SHFs over the GoL has been analyzed in this nonstationary mesoscale context. During periods of well-established Mistral/Tramontane winds, the mesoscale variability of LHFs and SHFs was controlled by the position of sheltered regions in the lee of the three major mountain ranges surrounding the GoL. A reduction of the order of 40% in LHF was observed and simulated between the jet and the sheltered regions. The impact of sheltered regions on the SHF field was not as marked as on the LHF field. During the period of established Mistral, both winds and vertical moisture (temperature) gradients controlled moisture (temperature) exchanges. During the period of disrupted Mistral, the strong easterly flow associated with the deepening low generated a huge sheltered region in the lee of the Alps, over the GoL (1500 UTC). As a result, SHFs and LHFs over the entire GoL were reduced by a factor of 2, on average with respect to the established cases. Also, during that period, air-sea moisture exchanges were almost entirely driven by dynamics. In all cases, the position of the sheltered regions, which evolved with the synoptic conditions, was the key to a correct interpretation of multiplatform surface turbulent flux measurements made over the GoL on 24 March 1998.

21562202c, 2003, C2, Downloaded from https://agupubs.onlinelibrary.wiley.com/doi/10.1029/2001JC001040 by Cochrane France, Wiley Online Library on [05/06/2023]. See the Terms and Conditions (https://onlinelibrary.wiley.com/terms-and-conditions) on Wiley Online Library for rules of use; OA articles are governed by the applicable Creative Commons License

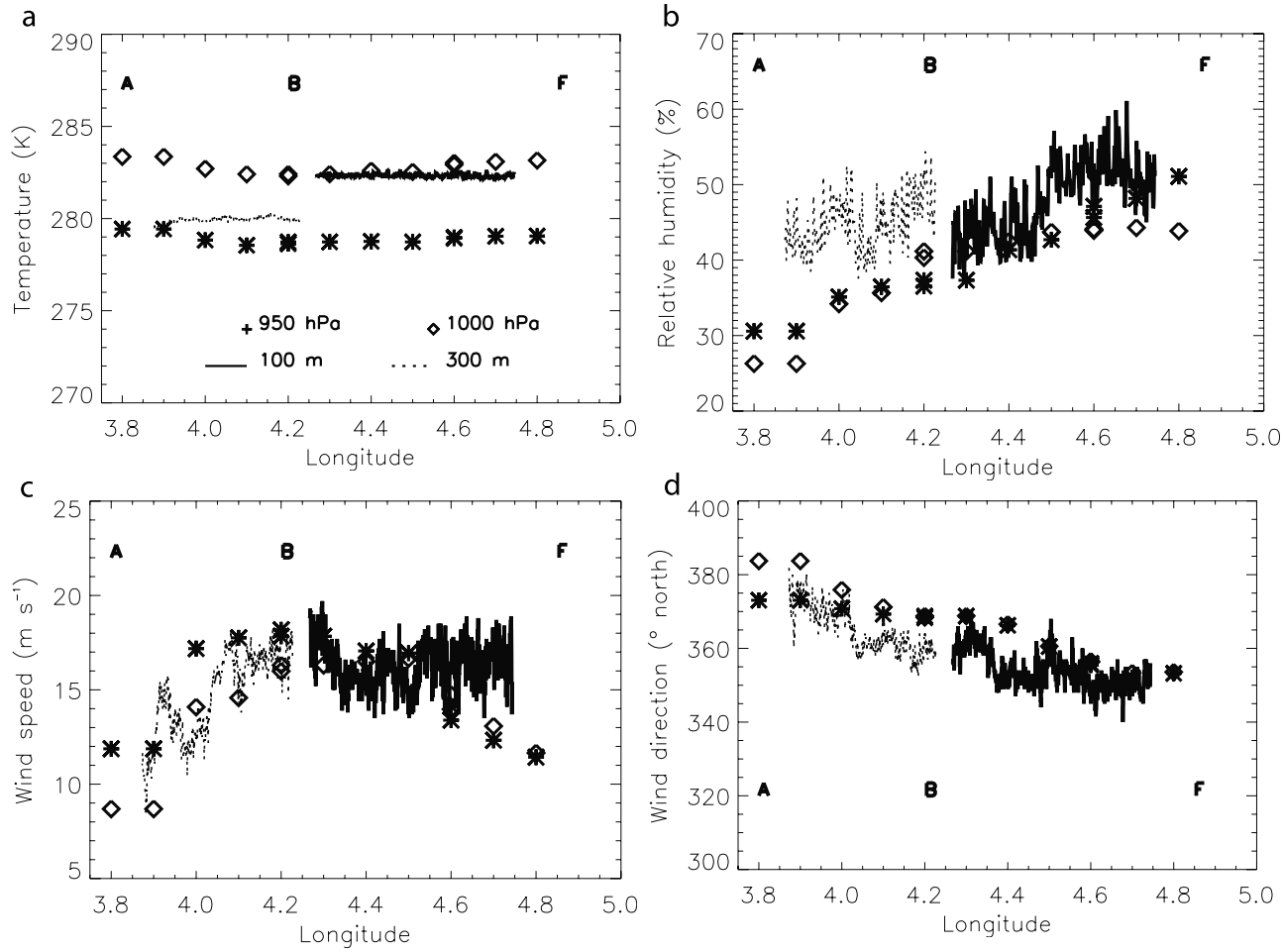

Figure A3. Comparison of (a) temperature, (b) relative humidity, (c) wind speed, and (d) wind direction extracted from the 1800 UTC ALADIN forecasts along leg AF at 1000 and 950 hPa (diamonds and asterix, respectively) with measurements made in the ABL by the ARAT on the same leg at 100 and 300 m (solid and dashed lines, respectively).

[50] The structure of the ABL over the GoL has been investigated by means of airborne laser remote sensing and in situ measurements during the established Mistral period and the disrupted Mistral period. In the latter period, lidar measurements show that in the region east of ≈4.4°E, the ABL depth decreased significantly (0.7 km instead of 1.2 km) and that fluctuations of the ABL top were reduced. This region coincided with that affected by the outflow from the Ligurian Sea on the 1800 UTC ALADIN forecast. It appeared that large directional wind shear at the top of the Mistral ABL connected to the outflow from the Ligurian Sea was responsible for preventing the Mistral ABL from developing. Furthermore, significant wave activity was observed during the established Mistral case, but not during the disturbed Mistral case.

[51] Finally, the confrontation of ALADIN forecasts to multiplatform measurements on the 24 March 1998 stressed out a few defects of the model (i.e., the early Tramontane event was not positioned properly). Nevertheless, ALADIN behaved remarkably well. More importantly, the spatiotemporal fluctuations of in situ mean and turbulent parameters along the aircraft and ship tracks and at the position of the buoy were consistent with the mesoscale picture provided by ALADIN.

[52] Further investigations of ABL oriented processes, namely (i) the influence of the Ligurian Sea outflow on the Mistral ABL structure, (ii) the origin of gravity waves as well as their influence of the ABL structure and possibly on air-sea exchanges and (iii) the role of sheltered regions (and associated potential vorticity banners), will be conducted using a mesoscale nonhydrostatic model.

Appendix: Comparison of ALADIN Simulations With Observations

[53] The objective was to estimate the reliability of the ALADIN simulations by comparing aircraft measurements and model outputs. We have selected representative parameters for ABL characterization: wind speed and direction, relative humidity and temperature. The measurements made by the ARAT in the ABL at 100 m and 300 m ASL are compared to ALADIN outputs at 1000 and 950 hPa. Note that, for the 1200 UTC forecast, pressure levels 1000 and 950 hPa correspond approximately to 163 and 584 m,

21562202c, 2003, C2, Downloaded from https://agupubs.onlinelibrary.wiley.com/doi/10.1029/2001JC001040 by Cochrane France, Wiley Online Library on [05/06/2023]. See the Terms and Conditions (https://onlinelibrary.wiley.com/terms-and-conditions) on Wiley Online Library for rules of use; OA articles are governed by the applicable Creative Commons License

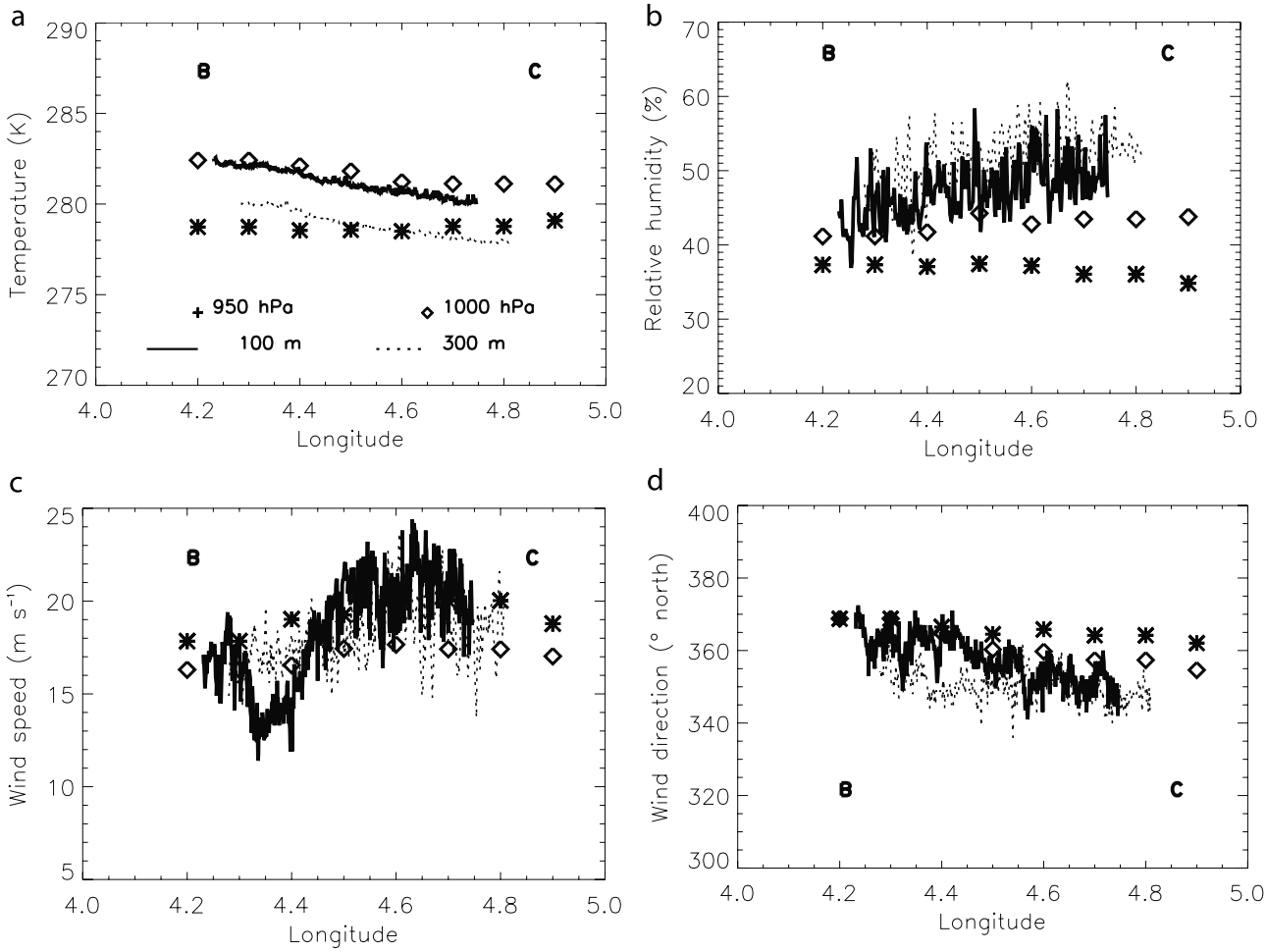

Figure A4. Same as Figure A3 but for leg BC.

respectively (Table 1). For the 1800 UTC forecast, pressure levels 1000 and 950 hPa correspond approximately to 186 and 609 m, respectively (Table 1).

A1. Well-Established Mistral Case

[54] We have proceeded to compare ALADIN outputs and ARAT in situ measurements on legs DE and BC. For the sake of clarity we present the comparisons on each leg on separate Figures. In this case, the agreement between forecast and measurements is impressively good. According to Figure 5, legs DE and BC ran across the western edge of the sheltered region, way points E and C being located in the core of the Mistral.

[55] Along leg DE (Figure A1), the wind direction, wind speed, RH and potential temperature are well reproduced by the model. Along leg BC (Figure A2), the wind direction, RH and potential temperature are also well simulated. However, it seems that the wind speed gradient across the region separating the sheltered area (in way point B) and the Mistral (between 4.2 and 4.5°E) is too pronounced.

[56] Most importantly, the thermodynamics across the transition from the sheltered region to the Mistral was documented during this flight. Measurements highlighted the following general characteristics across the western edge of the Mistral (going eastward): a change in wind direction from north to north-northwest, an increase in wind speed and a decrease in potential temperature. The amplitude of the changes were not observed to the same on legs DE and BC, most likely because way point B was located further west into the Mistral than suggested by ALADIN. RH trends on both legs were also observed to be opposite. However, low level convergence (between the Mistral and the Tramontane) at way point D may explain the rather high RH values observed.

A2. Perturbed Mistral Case

[57] According to Figure 5, leg AF ran across the Mistral, way point A being located in the eastern edge of the sheltered region, way point F in the eastern edge of the Mistral (the region to the east of the Mistral jet in which the wind speed decreases) and way point E being located in the sheltered region. Along leg BC, the ARAT sampled the ABL in a region of relatively constant winds in the Mistral.

[58] Along leg AF (Figure A3), wind speed was observed to increase from the coast (between 11 and 16 m s^{-1}) and reach a maximum at about 4.1°E. Between 4.1 and 4.75°E, the wind speed was observed to be nearly constant and equal to 16 m s^{-1}. All of this was consistent with ALADIN, except for the observed constant wind speed region (between 4.5 and 4.75°E) which is not predicted by the model. Measurements seem to indicate that the Mistral

21562202c, 2003, C2, Downloaded from https://agupubs.onlinelibrary.wiley.com/doi/10.1029/2001JC001040 by Cochrane France, Wiley Online Library on [05/06/2023]. See the Terms and Conditions (https://onlinelibrary.wiley.com/terms-and-conditions) on Wiley Online Library for rules of use; OA articles are governed by the applicable Creative Commons License

maintained its jet-like characteristics further southeast that suggested by ALADIN at 1800 UTC. The change in wind direction observed is well reproduced by the model. Along leg BC, ALADIN evidenced the presence of a low level jet (corresponding to the Mistral) at 950 hPa, in good agreement with the measurements at 100 m (Figure A4). At 100 and 300 m, the winds were stronger in the middle of the leg, in accordance with ALADIN (i.e., the flight track is closest to the 20 m s^{-1} isotach near 4.6°E). The wind speed also was correctly reproduced by ALADIN.

[59] Along leg AF, measurements suggested an increase of RH with longitude which is reproduced by ALADIN. At 1000 hPa, the RH increases from 25 to 45%, in fair agreement with the ARAT measurements, even though slightly underestimated by as much as 10%. Along leg BC, RH measurements indicate a slight increase with longitude from 40 to 55%. Simulated values are underestimated with respect to the measured ones.

[60] Temperature was observed to be relatively constant in the sheltered region (west of B). An important increase of the potential temperature (by 2 K) with the distance from the coastline was observed on legs BC (100 m ASL) and CB (300 m ASL), while on leg BF (300 m ASL), the potential temperature was observed to be constant. These fluctuations are well reproduced by the model.

[61] **Acknowledgments.** The author would like to thank Daniéle Hauser, who coordinated the FETCH experiment, Philippe Drobinski, Jacques Pelon, Stephanie Cosma, and Laurence Eymard for discussions, suggestions and comments. He is indebted to his colleagues who have participated to FETCH and, in particular, to Will Drennan for providing the ASIS buoy data, Pierre Durand and Hélène Dupuis for providing the airborne and ship-borne turbulent heat fluxes. Special thanks to Didier Bruneau, Vincent Trouillet, and Pascal Genau of Service d'Aéronomie; Frédéric Blouzon, Abdel Abchiche, Nadir Amarouche, Guy Pennazzi, Christian Allet, Noël Grand, André Gribkoff, and Bernard Sinardet of the Technical Division (INSU); Frédéric Marin (Météo-France) and Christine Guerin (Centre d'Etude des Environnements Plantaires). This research was funded by INSU/CNRS via the PATOM and PNTS programs.

References

Aebischer, U., and C. Schär, Low-level potential vorticity and cyclogenesis to the lee of the Alps, *J. Atmos. Sci.*, *55*, 186–207, 1998.

Alpert, P., M. Tsidulko, S. Krichak, and U. Stein, A multi-stage evolution of an ALPEX cyclone, *Tellus, Ser. B*, *48*, 209–220, 1996.

Bruneau, D., P. Quaglia, C. Flamant, M. Meissonnier, and J. Pelon, The airborne lidar LEANDRE 2 for water vapor profiling in the troposphere, Part I, Description, *Appl. Opt.*, *40*, 3450–3461, 2001a.

Bruneau, D., P. Quaglia, C. Flamant, and J. Pelon, The airborne lidar LEANDRE 2 for water vapor profiling in the troposphere, Part II, First results, *Appl. Opt.*, *40*, 3462–3475, 2001b.

Buzzi, A., and A. Tibaldi, Cyclogenesis in the lee of the Alps: A case study, *Q. J. R. Meteorol. Soc.*, *104*, 271–287, 1978.

Campins, J., A. Genoves, A. Jansa, J. A. Guijarro, and C. Ramis, A catalogue and a classification of surface cyclones for the western Mediterranean, *Int. J. Climatol.*, *20*, 969–984, 2000.

Drennan, W. M., H. Graber, D. Hauser, and C. Quentin, On the wave age dependence of wind stress over pure wind seas, *J. Geophys. Res.*, doi:10.1029/2000JC000715, in press, 2003.

Dupuis, H., P. K. Taylor, A. Weill, and K. Katsaros, Inertial dissipation method applied to derive turbulent fluxes over the ocean during the Surface of the Ocean, Fluxes and Interactions with the Atmosphere/Atlantic Stratocumulus Transition Experiment (SOFIA/ASTEX) and Structure des Echanges Mer-Atmosphere, Proprietes des Heterogeneites Oceaniques: Recherche Experimentale (SEMAPHORE) experiments with low to moderate wind speeds, *J. Geophys. Res.*, *102*, 21,115–21,129, 1997.

Dupuis, H., C. Guérin, W. Weill, P. Nacass, and D. Hauser, Impact of flow distortion corrections on turbulent fluxes estimated by the inertial-dissipation method during FETCH experiment on R/V *Atalante*, *J. Geophys. Res.*, doi:10.1029/2000JC001075, in press, 2003.

Egger, J., Numerical experiments on the cyclogenesis in the Gulf of Genoa, *Contrib. Atmos. Phys.*, *45*, 320–346, 1972.

Estournel, C., X. Durrieu de Madron, P. Marsaleix, F. Auclair, C. Julliand, and R. Vehil, Observation and modelization of the winter coastal oceanic circulation in the Gulf of Lions under wind conditions influenced by the continental orography (FETCH experiment), *J. Geophys. Res*, doi:10.1029/2001JC000825, in press, 2003.

Eymard, L., et al., Surface fluxes in the North Atlantic Current during the CATCH/FASTEX experiment, *Q. J. R. Meteorol. Soc.*, *125*, 3563–3599, 1999.

Eymard, L., A. Weil, D. Bourras, C. Guérin, P. Le Borgne, and J.-M. Lefèvre, Use of ship mean data for validating model and satellite flux fields during the FETCH experiment, *J. Geophys. Res*, doi:10.1029/2001JC001207, in press, 2003.

Flamant, C., and J. Pelon, Atmospheric boundary-layer structure over the Mediterranean during a Tramontane event, *Q. J. R. Meteorol. Soc.*, *122*, 1741–1778, 1996.

Flamant, C., et al., Airborne lidar measurements of aerosol spatial distribution and optical properties over the Atlantic Ocean during an European pollution outbreak of ACE-2, *Tellus, Ser. B*, *52*, 662–677, 2000.

Flamant, C., J. Pelon, L. Eymard, and J. Tournadre, SSM/I integrated water vapor content measurements in coastal regions: A comparison with shipborne and airborne remote sensing measurements, radiosonde measurements, and NWP model retrievals, *J. Geophys. Res*, doi:10.1029/2001JC001068, in press, 2003.

Graber, H., E. A. Terray, M. Donelan, W. M. Drennan, J. C. van Leer, and D. B. Peters, ASIS–a new air-sea interaction spar buoy: Design and performance at sea, *J. Atmos. Oceanic Technol.*, *17*, 708–720, 2000.

Grotjahn, R., and C.-H. Wang, On the source of air modified by surface fluxes to enhance frontal cyclone development, *Ocean-Air Interact.*, *1*, 257–288, 1989.

Hauser, D., H. Dupuis, X. Durrieu de Madron, C. Estournel, C. Flamant, J. Pelon, and P. Queffelou, La campagne FETCH: Une expérience pour l'étude des, échanges océan/atmosphère dans les conditions côtières du Golfe du Lion, *Météorologie*, *29*, 14–31, 2000.

Hauser, D., et al., The FETCH experiment: An overview, *J. Geophys. Res.*, doi:10.1029/2001JC001202, in press, 2003.

Hodur, R. M., The Naval Research Laboratory's Coupled Ocean/Atmosphere Mesoscale Prediction System (COAMPS), *Mon. Weather Rev.*, *125*, 1414–1430, 1997.

Kendall, M. G., and A. Stuart, *Advanced Theory of Statistics*, vol. 2, 2nd ed., Charles Griffin, London, 1967.

Lambert, D., and P. Durand, Aircraft to aircraft intercomparison during SEMAPHORE, *J. Geophys. Res.*, *103*, 25,109–25,123, 1998.

Louis, J.-F., M. Tiedtke, and J.-F. Geleyn, A short history of the operational PBL-parameterization at ECMWF, paper presented at the Workshop on Planetary Boundary Parameterization, Eur. Cent. for Medium-Range Weather Forecasts, Reading, England, 1981.

Marht, L., D. Vickers, J. Edson, J. Sun, J. Hojstrup, J. Hare, and J. Wilczack, Heat flux in the coastal zone, *Boundary Layer Meteorol.*, *86*, 421–446, 1998.

Powers, J. G., and M. T. Stoeling, A coupled air-sea mesoscale model: Experiments in atmospheric sensitivity to marine roughness, *Mon. Weather Rev.*, *128*, 208–228, 2000.

Trigo, I. F., T. D. Davies, and G. R. Bigg, Objective climatology of cyclones in the Mediterranean region, *J. Clim.*, *12*, 1685–1696, 1999.

C. Flamant, Service d'Aéronomie, Université Pierre et Marie Curie, Boite 102, 4 place Jussieu, 75252 Paris Cedex, France. (cyrille.flamant@aero.jussieu.fr)

21562202c, 2003, C2, Downloaded from https://agupubs.onlinelibrary.wiley.com/doi/10.1029/2001JC001040 by Cochrane France, Wiley Online Library on [05/06/2023]. See the Terms and Conditions (https://onlinelibrary.wiley.com/terms-and-conditions) on Wiley Online Library for rules of use; OA articles are governed by the applicable Creative Commons License